U.S. DEPARTMENT OF ENERGY

Sandia National Laboratories

SAND2017-10478R

SNL REPORT

SAND2017-zzzz

Printed September 26, 2017

Advancing Molten Salts and Fuels at Sandia National Laboratories—White Paper

By

Sal Rodriguez (Project Coordination, Editor)

Kenneth Armijo (Molten Salt Loop Test)

Brad Beeny, Matt Denman, Sal Rodriguez (Safety)

Ben Cipiti, Nathan Shoman, David Farley (Safeguards)

Sal Rodriguez (Computational fluid dynamics)

David Ames (Nuclear criticality safety, neutronics, MCNP)

Charles Andraka, Ronald Briggs, Richard Sisson, Kenneth Armijo, Sal Rodriguez (Meeting for pathway to restart MSTL)

Ken Armijo (LOFTED Facility and miscellaneous molten salt experiments)

Richard Sisson (2017 MSTL pictures)

Prepared by
Sandia National Laboratories
Albuquerque, New Mexico 87185 and Livermore, California 94550
R&A Tracking Number:

Programmatic Review, Gary Rochau

EXECUTIVE SUMMARY

Sandia National Laboratories is a multimission laboratory managed and operated by National Technology and Engineering Solutions of SNL, LLC., a wholly owned subsidiary of Honeywell International, Inc., for the U.S. Department of Energy's National Nuclear Security Administration under contract DE-NA0003525.

SNL has a combination of experimental facilities, nuclear engineering, nuclear security, severe nuclear accidents, and nuclear safeguards expertise that can enable significant progress towards molten salts and fuels for Molten Salt Reactors (MSRs). The following areas and opportunities are discussed in more detail in this white paper.

- Molten salt experiments—molten salt test loop (MSTL). This section includes a detailed discussion of molten salts applicable for MSR and solar applications. The emphasis is operation, chemistry, corrosion, and instrumentation. A description of MSTL, its capabilities, and level of effort required to restart the facility is presented, as well as innovative, potential upgrades for fluoride and chloride experiments, loop sectioning for multiple experiments, and fission surrogates. MSTL restart is estimated conservatively to cost $1/10^{th}$ the value of building a new facility. Furthermore, its large-scale operating regime continues to lead the industry.
- Safety. MELCOR can already model several types of advanced reactors, including VHTRs, water-cooled SMRs, and sodium-cooled reactors. Current MSR capabilities in MELCOR are discussed. This investigation identified several useful MSR capabilities that are straightforward to implement. For the longer term, advanced MSR models and safety issues are identified.
- Safeguards. An FY18 safeguards performance model for the Material Protection Accounting and Control Technologies (MPACT) program at DOE NE is described. Experiments using fission surrogates in molten salt mixtures are recommended for MSTL. A 2017 NA-241 safeguards analysis for thorium fuel indicates intense gamma radiation. However, this issue can be addressed at SNL's experimental facilities, and funding should be sought in this area as well.
- Computational fluid dynamics (CFD). CFD modeling at SNL includes state-of-the-art large eddy simulation (LES) using the dynamic Smagorinsky turbulence model and the direct numerical simulation (DNS) model. It is noted that SNL has used CFD to successfully model gas- and water-cooled fuel assemblies under forced and natural circulation, as well as molten salt surfaces under natural circulation. SNL also has excellent coupled Multiphysics codes that couple CFD with heat transfer and structural analysis.
- Nuclear criticality safety and neutronics. Because of its versatility and significant number of successful benchmark experiments, the Sandia Critical Experiments (SCX) facility is ideally suited to perform criticality experiments for molten salt-based fuels. SNL also has a broad-based experience in designing, performing, and analyzing critical benchmark experiments that will be invaluable assets for advancing molten salts and fuels.

The above are areas where SNL could submit proposals with a higher degree of success because they have the highest degree of synergism between SNL's technical expertise and the recent paradigm at DOE and ARPA-E. These organizations have recently acquired a stronger stake in advanced nuclear reactors, especially MSRs and SMRs.

1. INTRODUCTION

There is recent evidence that DOE and ARPA-E are taking a stronger interest and stake in innovative, advanced reactor concepts. These advanced concepts include the utilization of heat pipes, advanced molten salts (both chlorides and fluorides), small modular reactors, and novel breeding techniques. This is consistent with the recent Advanced Non-Light Water Reactor Workshops conducted over the past three years by the DOE and NRC in Washington, DC. But more compellingly, the DOE recently funded advanced reactor research that is outside the norm of the 10 years, including innovative research that is generally considered riskier due to perceived technological gaps. For example, in 2016, the DOE awarded TerraPower and its partners (ORNL, Southern Company, Vanderbilt University, and EPRI) a $40 million contract spread over five years, to develop a molten chloride fast reactor (MCFR) [Bushey, 2017]. This is a significant paradigm shift for DOE, as fluoride salts have a stronger basis than chlorides in molten salt reactors that have been built previously (e.g., Molten Salt Reactor Experiment, Aircraft Reactor Experiment). It is significant that TerraPower not only continues to work on a heat-pipe traveling wave reactor, but is also working on an MCFR design. Further, ARPA-E has expressed a desire to seek innovative nuclear solutions that have higher rewards, albeit at a higher risk.

As expressed in a recent report [Rodriguez, 2017],

> "ARPA-E's mission is to foster innovation and revolutionary advances in science and energy. It therefore funds high-risk, high reward research that often goes unfunded by industry."

Though ARPA-E has applied the above strategy to fusion and non-nuclear energy such as coal, wind, and solar, it, too, is showing a paradigm shift in favor of advanced, innovative nuclear fission reactors. This is reflected in ARPA-E's "Safe and Secure Megawatt-Size Nuclear Power Workshop" that was held in Washington DC [Megawatt Workshop, 2016], as well as the recent request for information (RFI) (RFI-0000031, "Announcement of Teaming Partner List for an Upcoming Funding Opportunity Announcement: Designs for Advanced Modular Nuclear Reactors") [RFI, 2017]. To further strengthen this position, it is noted that Ji-Cheng (JC) Zhao, the ARPA-E Program Director, views nuclear power's future as strongly based in SMRs, with clear advantages based on its minimal CO2 footprint. He also considers SMRs as ideal for on-site manufacturing and certification, micro-grids, critical infrastructure, military installations, space, maritime, and remote areas [Zhao, 2016].

Thus, there is ample evidence that the obstacles for implementing innovative advanced reactor concepts are starting to disappear. Curiously, many of the concepts that were adopted and embraced in the 50s and 60s are now re-emerging. Therefore, Sandia National Laboratories (SNL) now has a unique opportunity to provide relevant services and research in areas where it has traditionally led and provided substantial expertise. For molten salts and fuels, this includes the following areas:

- Section 2: Molten salt experiments at the Molten Salt Test Loop (MSTL)
- Section 3: Safety
- Section 4: Safeguards
- Section 5: Computational fluid dynamics (CFD)
- Section 6: Nuclear criticality safety and neutronics
- Appendix A: LOFTED Facility
- Appendix B: Miscellaneous molten salt experiments at SNL (corrosion, thermal storage)

In this white paper, the above areas are examined to characterize SNL's current technical capabilities related to molten coolants and fuels. This investigation identifies and ranks SNL's strengths and weaknesses, for the purpose of increasing our competitiveness. Recommendations for improvement and paths forward are included.

2. MSR EXPERIMENTS—MOLTEN SALT TEST LOOP (MSTL)

For concentrating solar power (CSP) applications the most profound advantage of molten salts employed a heat transfer fluid (HTF) is the possibility of direct storage at relatively low costs. Commonly used nitrate salts (60% NaNO3 and 40% KNO3 by mass) are stable to relatively high temperatures of up to 600 °C though their lower maximum temperature can be limiting as further increased temperatures increases the corrosion rate with stainless steels (SS) [3]. Generally, heat transfer characteristics of molten salts are mediocre where a reasonably high density and low specific heat capacity enable a low volume flow but the low thermal conductivity can lead to elevated thermal losses [4]. The high solidification temperatures of liquid salts can present challenges where the HTF could freeze during evening hours or during times of low solar irradiance [4]. In central receiver systems, molten salt will normally be drained into a tank during receiver filling with a cover gas, though the freezing of the salt, which could block pipes and valves, could cause severe damage to a system [7]. Just as with molten metals, solutions to freezing, aside from draining, could include trace heating or circulation of stored salts. However, these solutions could result in higher heat losses, electrical power consumption and investment costs. Research has been conducted to address this issue for the development of salts with lower melting points [4], as well as higher maximum operating temperatures to facilitate higher efficiency power cycles [7]. Advanced salt concentrations have previously been studied in an effort to raise the power cycle operating temperatures. Raade et al. [10] found a quinary composition of LiCl, NaCl, KCl, CsCl and SrCl to have a melting point of 253 °C at ambient pressure, and a thermal stability of up to approximately 750 °C. Earlier studies have previously been performed to understand molten salt thermal-fluid behavior in advanced CSP molten salt power generation applications [11, 12]. Hoffman [13] investigated turbulent heat transfer for molten NaOH for Reynolds number (Re) values of 6,000 to 12,000 where the authors determined heat transfer characteristics followed the correlation:

(1) $$Nu = 0.021 Re^{0.8} Pr^{0.4}$$

A wider range of Re was studied by Grele and Gedeon [14] between 5,300 to 30,000, where the authors measured values of Nu were 20% higher than those of the widely-used Dittus-Boelter equation, Eqn. 2.33. Hoffman and Cohen [15] studied molten NaNO2-NaNO3-KNO3 for heat transfer for Re between 4,850 and 24,710 and between heat flux up to 614 kW/m^2, where the authors also found good agreement between their data and the Dittus-Boelter equation. In another study, Yu-Ting et al. [16] researched molten LiNO3 salt flowing through a test section that rejected heat to a cooling oil flowing a jacket around a test section with a Re range 4100-9850 where the authors showed good agreement between their experimental data and the Gnielinski equation [17] and the Hausen equation [16]. Additionally, a study by Das et al. investigated molten nitrate salt [10] (60% NaNO3 and 40% KNO3) up to Re values of $2x10^5$ and heat flux levels up to 1,000 kW/m^2. The authors found good agreement between their developed Nu correlation and their data, where two major effects were observed: 1. the Nu values gradually plateaued for the highest Re tested and 2. at higher Re values, positive interaction of heat flux on Nu was observed [10].

2.1. Nitrate Salts

Significant data exist regarding thermophysical properties (heat capacity, density, viscosity, and thermal conductivity) and corrosion performance of alloys up to about 620 °C, which is believed to represent the practical upper temperature limit for nitrate salts [Gen III roadmap]. Some data suggest this temperature limit could be increased by stabilizing the nitrate anion with a high-oxygen-content ullage gas [Gen3 roadmap ref 6]. Although nitrates may be able to operate at higher temperatures than currently deployed, it is understood that nitrates will not reach temperatures that are necessary to achieve SunShot power cycle efficiency goals, (i.e. ≥ 700 °C) [Gen3 roadmap ref 8]; thus, a different salt chemistry is required for enhanced CSP systems. Candidate salts must have favorable thermophysical properties for heat transfer and energy storage (e.g., low melting point, high heat capacity, high thermal conductivity), chemical stability, chemical compatibility with sCO2 Previous analysis has shown that candidate salts have been identified, where each has been reported to be stable up to around 800 °C. The onset decomposition of the eutectic Na2CO3/K2CO3/Li2CO3 under a CO2 blanket has been reported to be above 1,000 °C with weight loss due to salt evaporation starting at 788 °C. Under air, the decomposition was reported at 601°C with a rapid rate of weight loss at 673 °C [Olivares, Chen, and Wright, 2012]. Volume change on melting, an important criterion for freeze recovery, is reported in Table 1.

Table 1. Candidate molten-salt heat-transfer fluids and approximate physical properties, or for the pure components if mixture data are not available [28].

Salt	Composition by Wt.	Melting Point (°C)	Heat Capacity (J/g-K)	Density (kg/L)	Δ Volume on Melting	Notes**	Ref.
$NaNO_3$ KNO_3 (baseline)	0.60 0.40	220	1.52	1.7	+4.6%		[10]
$ZnCl_2$ NaCl KCl	0.686 0.075 0.239	204	0.81	2.4	NaCl/KCl: +14.8% [11] NaCl: +26.1% KCl: +22.3% [11]	ZnCl BP(732°C) [12]	[13]
$MgCl_2$ KCl	0.375 0.625	426	1.15	1.66	KCl: +22.3% $MgCl_2$: +30.5% [11]	$MgCl_2$ BP(1412°C)	[14]
Na_2CO_3 K_2CO_3 Li_2CO_3	0.334 0.345 0.321	398	1.61	2.0	+3.6% [11]	EP(747°C) 0.014 atm EP(827°C) 0.041 atm EP(947°C) 0.151 atm [9] [12]	[13] [15]
**BP(XXX°C): boiling point temperature, EP(XXX°C): equilibrium pressure at a given temperature of CO_2							

While this realm of stability depends on many factors (i.e. pressure, temperature, presence of various cations, time at temperature, free surface available for reaction, impurity concentrations, etc.) nitrate salts will likely not be able to push toward the aggressive temperatures needed for economic viability of solar thermal. Temperatures of 700-800 °C are being projected to fully utilize Advanced Supercritical Carbon Dioxide (sCO2) Brayton Cycles [Stekli, 2011]. In most situations as temperature is increased the corrosive behavior of the fluid increases in an Arrhenius fashion. Mechanisms of corrosion must be well understood in order to discern and strategically focus precious time and resources available for research [Stekli, 2011].

2.2 Lithium Salts

Salts containing lithium have also been studied for thermal energy storage (TES) systems applications because of their optimal thermophysical properties. Lithium nitrate has been considered as a great additive to improve the thermal performance for sensible heat storage of molten salts, due to its ability to increase the salt mixture's working temperature range [18]. In their research, Fernández et al. [19] characterized thermophysical properties of lithium nitrate containing salts with corrosion evaluations of carbon and low chromium steels at 390 °C for 1000 hours. Thermophysical properties, such as melting point, heat capacity and thermal stability of saline nitrates were measured using a simultaneous thermogravimetric analyzer (TGA) and differential scanning calorimeter (DSC), which included NaNO3 and KNO3 (SQM-SSR grade), $Ca(NO_3)2*4H_2O$ and $LiNO_3$ (Panreac 98%) [19]. Their results, as shown in Table 2, showed that using lithium and calcium nitrate, in small quantities (10 wt. %), enabled the salt mixture energy density to increase by 19%. Their results also found a reduction in thermal stability due to the

incorporation of corrosion products into the salt. A steep reduction in weight % was observed around 350 °C in the salts after the corrosion tests.

Table 2. Thermophysical properties of lithium nitrate containing molten salts [19].

Molten salt mixture (wt.%)	Work temp. range (°C)	Viscosity at 250°C (cP)	Corrosion rate of A516 Steel at 390°C (mm/year)	Electrical conductivity at 390°C ($\Omega^{-1}m^{-1}$)	Energy density (MJ/m^3)	Salt Price (US$/Ton)	Two-tanks system cost/stored energy (US/kWh_{th}$)
Solar Salt	221–589	5.51	0.97	0.37	550	893	11.67
20 $LiNO_3$ – 52 KNO_3 – 28 $NaNO_3$	130–600	6.3	0.31	0.67	513	1161	16.35
30 $LiNO_3$ – 10 $Ca(NO_3)_2$ – 60 KNO_3	134–567	5.72	0.027	0.56	607	1274	15.07
10 $LiNO_3$ – 10 $Ca(NO_3)_2$ – 60 KNO_3 – 20 $NaNO_3$	132–580	5.78	0.013	0.45	680	1038	10.98

2.3 Chloride Salts

Chloride salts also have the potential for being excellent candidates as HTFs for CSP considering how they can operate at much higher temperatures than nitrate salts, however they are susceptible to high corrosion rates in the presence of moisture and oxygen. Purification techniques however can be employed to ensure formation of protective layers do not readily occur where ullage gas may also be employed to reduce corrosion, though a study by Kruzenga [24] showed that oxygen content must be lower than 10%. Impurities in the form of oxygen and moisture are much less of an issue in carbonate salts. For carbonate salts ullage gases are typically high in CO_2 content, where formation of protective oxide layers has been found to inhibit corrosion from the base alloy [24]. Additionally, Ren *et* al. [26] and Olivares *et* al. [27] proposed replacing molten nitrate salts with mixed carbonate salts since their corrosion-reducing ability could further increase operation temperatures to between 700 °C and 850 °C. Research by de Miguel *et* al. [25] investigated corrosion behavior of an austenitic steel HR3C in a eutectic ternary carbonate molten salt mixture ($Na_2CO_3/K_2CO_3/Li_2CO_3$) through an isothermal immersion test at 700 °C for 2000 hrs. A microstructural and compositional study was performed using SEM – EDX and XRD analysis where they observed corrosion products arranged in a multilayer structure, with $LiFeO_2$, $LiCrO_2$, NiO and $FeCr_2O_4$ being the main compounds in different layers (from molten salt to the unaffected substrate interface). The weight loss observed through gravimetric analysis was attributed to soluble chromates initially formed (K_2CrO_4). Despite this weight loss the utility of carbonate steels in CSP applications still appears promising, however further research over longer time periods at high temperatures (about 700 °C) is still required to ensure compatibility of carbonate salts that the HR3C steels [25], as well as other CSP materials.

To address corrosion issues, especially with chloride salts which are extremely corrosive to stainless steels, nickel alloys can be employed, however their costs can be prohibitive. However, chemically resistant coatings can also be applied to ensure system internal surfaces

have low wettability and can withstand long-term exposure to these materials at temperatures greater than 600 °C [23]. When power turbines and containment alloys reach temperatures greater than 700 °C, the salts form a thin film of molten fluid that attacks the substrate metal alloy (hot corrosion). The applied coatings are designed to limit degradation of the underlying substrate [20, 21] where they must be very dense with minimal defects during application to ensure good resistance [22]. Protective coatings are formulated to corrode at an established rate (µm/yr. normal to the surface) when in contact with the HTF. This corrosion rate determines the coating thickness that is required to protect the substrate for a 30-year lifetime of a respective plant. To protect storage tank walls and piping from corrosion and eventual failure, coatings are being developed that have a target corrosion rate of 30 µm/yr. with a minimal thickness of 900 µm [23].

2.4 Carbonate Salts

Alkali carbonate salts are used in molten carbonate fuel cells (MCFC) at temperatures around 650°C [28]. Low-lithium salt blends may have acceptable physical properties for use as a solar HTF and reduce cost; for example, some researchers have reported carbonate salt blends having only 10% lithium carbonate and maintaining acceptable thermophysical properties [29, 30], although these results need to be validated. The composition of the carbonate blend should be optimized for cost by determining if limiting the lithium salt content will significantly impact other salt properties (e.g., density, heat capacity, melting point). 2O, and CO_2 as part of operation, and they are inherently less corrosive than chloride salts under such conditions. Not requiring an inert headspace provides a distinct advantage. Although corrosion is still an issue of concern, the greatest potential problem with the eutectic carbonate salt blend is the cost of lithium carbonate. Related to cost, a major concern with respect to carbonates is the supply of lithium carbonate in view of the demand for lithium in the growing battery market. A 10-MWe demo plant with 10 hrs. storage would require 350 metric tons (MT) of lithium carbonate, whereas a 100-MWe plant would require 8,000 MT. Lithium carbonate production in 2015 was about 153,000 MT [31]. The expected increase in lithium demand for batteries, combined with the potential for new lithium production sources, create uncertainty in the future price of lithium carbonate. This potential market spurs pursuit of other sources of lithium and market analysts have projected scenarios leading to increases or decreases in lithium price. For example, some geothermal plants are working to produce lithium compounds as a byproduct [28]. Lithium from these domestic sources could be a significant advantage for greater use of lithium in U.S. industry. Lastly, physical property data exist for solar salt over the range of its normal operating conditions of 300 °C to 600 °C [32], however there is not a similar level of knowledge for carbonates and chloride salts. Accurate physical property data (e.g., heat capacity, viscosity, density, thermal stability, thermal conductivity) are important for the design of piping and heat exchangers. These data should be developed, validated, and published for the candidate salt compositions.

2.5 Fluoride Salts

Liquid-fluoride-salt has previously been proposed to raise the heat-to-electricity efficiencies of solar power towers, Figure 1 to about 50% [33] where molten salt would deliver heat from the solar furnace at temperatures between 700 and 850 °C to a closed multi-reheat Brayton power cycle using nitrogen or helium as the working fluid. During the daytime, hot salt may also be used to heat graphite, which would then be used as a heat storage medium to make night-time operations possible. Graphite is a low-cost high-heat capacity solid that is chemically compatible with liquid fluoride salts at high temperatures. About half the cost of a solar power tower is associated with the mirrors that focus light on the receiver, and less than one-third is associated with the power cycle and heat storage [33]. Consequently, increasing the efficiency by 20–30% has the potential for major reductions in the levelized cost of electricity (LCOE). Peak temperatures and efficiencies of current power tower designs are restricted by: A. the use of liquid nitrate salts that decompose at high temperatures and B. steam cycles in which corrosion limits peak temperature. The liquid-fluoride-salt technology and closed Brayton power cycles are being developed for high-temperature nuclear reactors [34] which may provide technology and an industrial basis for an advanced solar power tower. As in the case of fluoride salts, the identification and testing of redox buffers to suppress corrosion of the container alloy is highly desirable and may be absolutely necessary for operation of the heat-transfer loop at the highest temperatures with other halide salts [35].

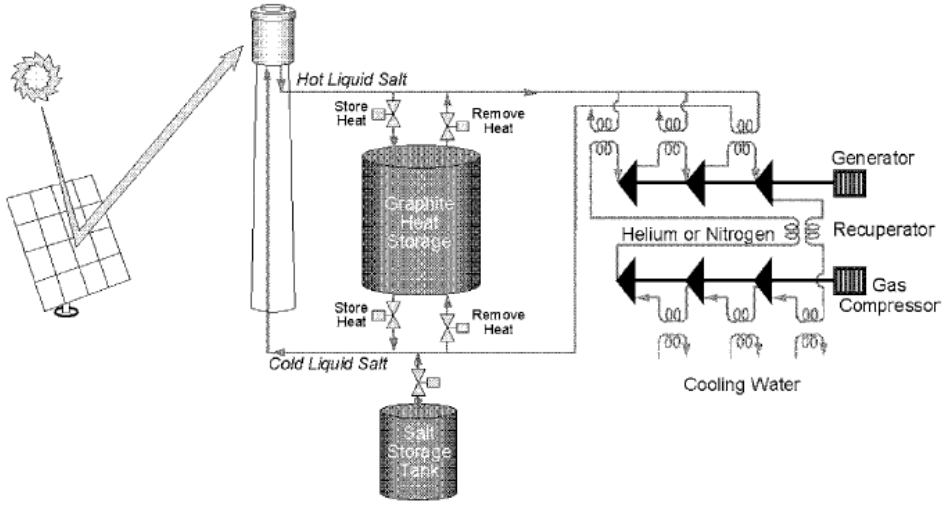

Figure 1. Solar power tower with liquid-salt heat transport system, graphite heat storage, and Brayton power cycle [33].

Table 3. Summary of the properties of candidate coolants for the NGNP/NHI heat-transfer loop [35].

Salt	Formula weight (g/mol)	Melting point (°C)	900°C vapor pressure (mm Hg)	Heat-transfer properties at 700°C			
				ρ, density (g/cm^3)	ρ^*Cp, volumetric heat capacity (cal/cm^3-°C)	μ, viscosity (cP)	k, thermal conductivity (W/m-K)
LiF-NaF-KF	41.3	454	~0.7	2.02	0.91	2.9	0.92
NaF-ZrF_4	92.7	500	5	3.14	0.88	5.1	0.49
KF-ZrF_4	103.9	390	1.2	2.80	0.70	< 5.1	0.45
LiF-NaF-ZrF_4	84.2	436	~5	2.92	0.86	6.9	0.53
LiCl-KCl	55.5	355	5.8	1.52	0.435	1.15	0.42
LiCl-RbCl	75.4	313	--	1.88	0.40	1.30	0.36
NaCl-$MgCl_2$	73.7	445	< 2.5	1.68	0.44	1.36	0.50
KCl-$MgCl_2$	81.4	426	< 2.0	1.66	0.46	1.40	0.40
NaF-$NaBF_4$	104.4	385	9500	1.75	0.63	0.90	0.40
KF-KBF_4	109.0	460	100	1.70	0.53	0.90	0.38
RbF-RbF_4	151.3	442	< 100	2.21	0.48	0.90	0.28

Liquid fluoride salts are excellent high-temperature HTFs. Table 3 shows the properties of several liquid fluoride salts and other coolants, including the typical nitrate salt used in current power tower designs. In all cases, binary or more complex fluoride salt mixtures are preferred because the melting points of fluoride salt mixtures are much lower than those for single-component salts. Many other properties, such as vapor pressure, density, thermal expansion coefficient, and viscosity can also be modified with the appropriate salt mixture to produce more desirable qualities.

Table 4. Characteristics of CSP HTFs and Graphite [35].

Coolant	T_{melt} (°C)	T_{boil} (°C)	ρ (kg/m^3)	C_p (kJ/kg°C)	ρC_p (kJ/m^3°C)	K (W/m°C)	$v \cdot 10^6$ (m^2/s)
LiF–NaF–KF (46.5–11.5–42)	454	1610 (est)	2020	1.89	3820	~0.6–1	1.4
NaF–$NaBF_4$ (8–92)	385	700[b]	1750	1.51	2640	0.5	0.5
$NaNO_3$–KNO_3[c] (66.3–33.7)	221	c	1772	1.53	2710	0.53	
Sodium	97.8	883	790	1.27	1000	62	0.25
Lead	328	1750	10,540	0.16	1700	16	0.13
Helium (7.5 MPa)			3.8	5.2	20	0.29	11.0
Water (7.5 MPa)	0	290	732	5.5	4040	0.56	0.13
Graphite			1700	1.9	3230	200	

As shown in Table 4, with some three- and four-component mixtures, it is possible to reduce melting points to approximately 300°C. At operating conditions, the thermophysical properties of liquid salts are similar to those of room temperature water except for the very low vapor pressure of many liquid fluoride salts. Fluoride salts are thermodynamically stable at high temperatures with very high boiling points. Liquid fluoride salts do not react with helium or nitrogen but will react slowly with water. According to Forsberg [33] there are several candidate salts, where the selection of a specific fluoride-salt depends upon the particular application and requirements. Solar power towers do not have nuclear requirements such as low nuclear cross

sections for capture of neutrons; thus, a wider choice of fluoride-salts exists for such applications. To avoid corrosion, liquid-fluoride-salt coolants must be thermodynamically stable relative to the materials of construction; that is, the materials of construction must be chemically noble relative to the salts. This requirement is necessary because fluoride salts are fluxing agents that rapidly dissolve protective layers of oxides associated with many metals, thus limiting the choice to highly thermodynamically stable salts if metal alloys of construction are to be used [33].

Figure 2 demonstrates that, in general, optimized compositions of fluorides have the lowest vapor pressure, followed by chlorides, and then fluoroborates. Potassium fluoroborate has a much lower vapor pressure at 900 °C (about 0.13 atm) and is a better choice for the heat-transfer-loop application. The pressure of potassium fluoroborate at 900 °C is approximately equal to the vapor pressure of sodium fluoroborate at 620 °C [35].

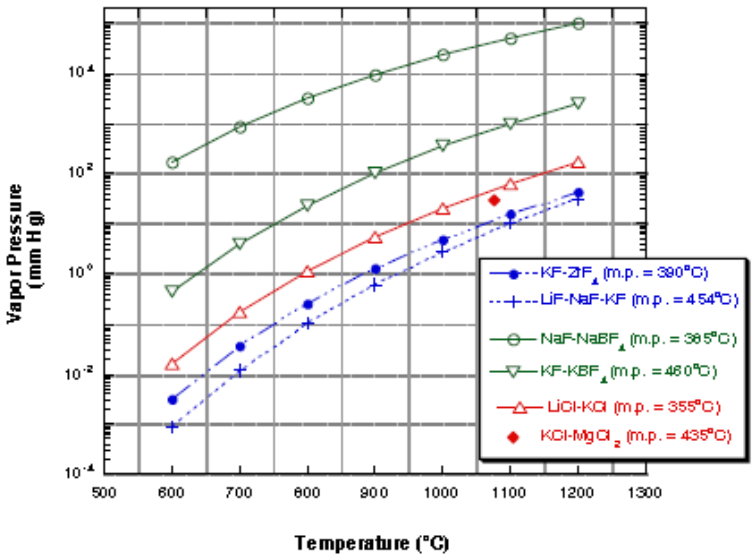

Figure 2. Vapor pressure of selected candidate molten salts [35].

Increasing the peak coolant temperatures and using a higher-temperature closed-Brayton-power cycle have the potential to increase heat-to-electricity efficiency by 20–30% with an equivalent reduction in capital costs [33]. The fluoride salts are thermodynamically stable (i.e., they do not decompose upon heating) and have atmospheric boiling points above 1000 °C [33]. For a system using fluoride salts, the preferred heat-storage medium is graphite. Graphite is a relatively low-cost high-temperature heat sink that is chemically compatible with the salt. While the salt could be used to store heat, it is more expensive than graphite [33]. When the solar power tower is operating with thermal output that exceeds the requirements for the power conversion unit, hot salt flows downward through channels in the graphite, heats the graphite, and returns to the power tower. When the solar power tower is not operating and heat is required, salt flows upward through coolant channels in the graphite, is heated, and then flows to the power conversion unit. For these systems the working fluid may be nitrogen or helium [33].

2.3 Molten Salt Test Loop (MSTL)

2.3.1 MSTL Overview

The molten salt test loop (MSTL) was designed to allow industrial customers and researchers to test molten salts over a range of temperatures within energy-generation individual components such as flex hoses, ball joints, and valves, up to full solar collecting and heated systems. However, these values can be increased or decreased depending on the pump curve at the desired operating point. As shown in Figure 3, the system has 3 parallel test loops, made from 345H stainless steel, that provide locations where a customer's experiment can be attached for testing in flowing salt in plant-like conditions.

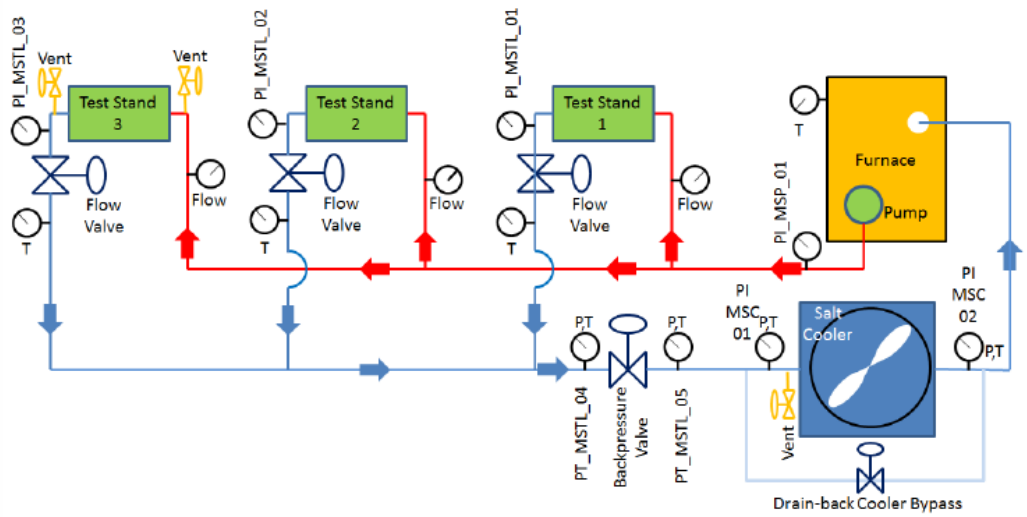

Figure 3. Flow schematic for the molten salt test loop showing flow and pressure meters [37].

The available salt temperature for this loop is 300-585 °C (572-1085 °F) for the 3 individual loops, as shown in Figure 4. The salt temperature is controlled by electric immersion heaters in the furnace (240kW) where the test system can accept and remove up to 1.4 MW_{th} input from the system by either pump work or by heat input from the experiment. The facility currently uses a 60/40 nitrate "solar salt" and can circulate the salt at pressure up to 40 bar (600psi), temperatures up to 585°C, and flow rates of 44-50 kg/s (400-600gpm) depending on temperature, for each of the three test loops [37]. The system is designed to gravity-drain back to the furnace upon loss of pump pressure and the piping and valves are fully heat traced to prevent salt freeze-up on system fill. There is an adjacent, temperature controlled building which contains the system control computer and the data acquisition system which has the capability to collect data from both the MSTL system as well as from customer's experiments.

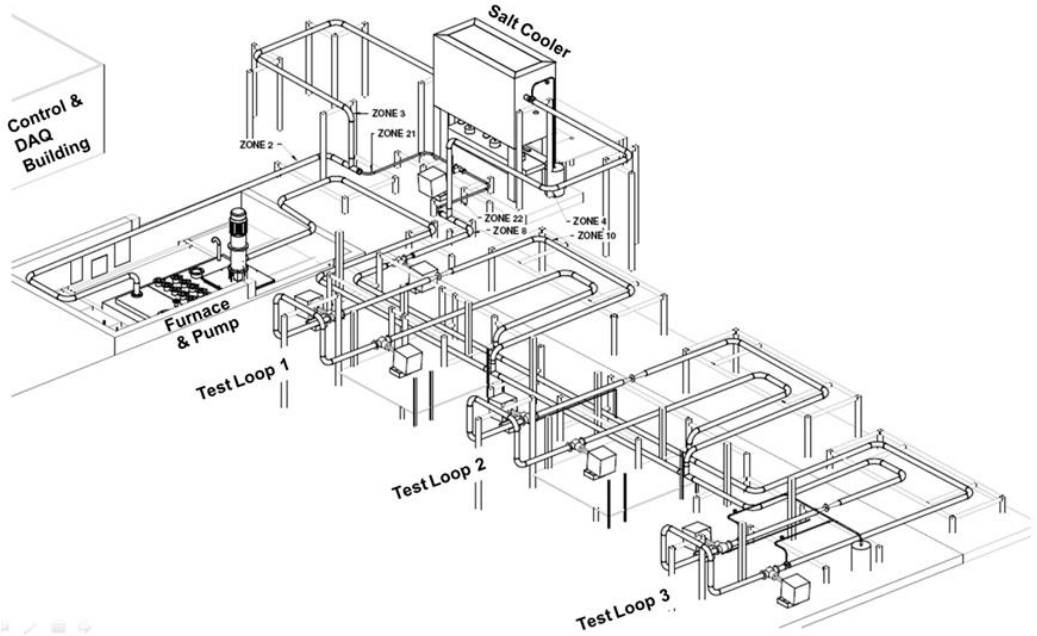

Figure 4**.** MSTL Isometric view showing system hardware and test stands [38].

For this capability, nitrate salts have traditionally been tested composed of either a sodium nitrate/potassium nitrate mixture (near the eutectic point) or a sodium/potassium/calcium nitrate eutectic. These salts are typically used to a maximum temperature of 585 °C because of a nitrate/nitrite disassociation that occurs more rapidly above this temperature. Though this reaction is reversible, often the oxygen from the dissociation creates metal-oxides with the fluid handling piping/tankage/pumps/valves and thus corroding the equipment. However, there are still challenges that must be solved before either chloride, fluoride or carbonate salts can be tested at MSTL. In either the 585 °C nitrate salt case or the >650 °C carbonate, fluoride or chloride cases, there is a significant challenge regarding pressure and flow instrumentation as well as cover gas selection, and leakage detection.

2.3.2 MSTL Technology for Flow and Pressure

The maximum available salt pressure is 40 bar and is set by the pump and the backpressure control valve. The flow rate is set primarily by the pump and the flow control valves on the outlet of each test stand. The system is designed to provide uninterrupted flow for tests up to 3000 hours with full capabilities for data collection and process monitoring. As shown in Figure 5, the MSTL pump is comprised of a 9-stage, stainless steel, vertical turbine pump manufactured by Flowserve, which is driven by a variable frequency drive that allows for a broad range of flow and pressure conditions in the experimental test loops. Additionally, the system has a rotary screw air compressor that has maximum capability of 132 psi and 38.6 cfm. Because of other air demands and piping losses, the experimenter can expect 50 psi air with a maximum usage rate of 20 cfm. This air is provided to the experimental test stand in 0.5 in. diameter tubing and has

a 0.5 in. quick-disconnect fitting for connection. Each test stand has a 0-50 psi gauge for monitoring of air pressure.

Anticipated experiments include flowing salt corrosion tests and accelerated life testing of components for both CSP and other molten salt applications, which could include Nuclear energy, among other industrial thermal storage systems. The maximum amount of molten salt that may be dedicated to any one test article without affecting the performance of other test articles inserted in the other two loops is approximately 800 gallons.

Initially a set of tests were conducted to evaluate the use of pressure sensors for flow measurements across devices of known flow coefficients, C_v. Pressure indicators for molten salts are severely affected by system conditions, where pressure changes of nearly 200 psi were evident during the tests when there was no flow or pressure in the system. Several iterations of performance improvements were undertaken and the pressure changes were reduced to less than 15 psi [38]. The results of the pressure improvements were then tested for use as flow measurements. It was later found that even with improved pressure sensors, it was not a reliable method of flow measurement. The need for improved flow and pressure measurement at high temperatures remains and will need to be solved before it will be possible to move to high temperature thermal storage systems with molten salts. Currently available flow and pressure instrumentation for molten salt is limited to 535 °C and even at this temperature the pressure measurement appears to have significant variability [38].

Figure 5. MSTL Flowserve Pump System [37].

2.3.3 Pressure Measurements

A Gefran pressure transducer was employed for experimentation, Figure 6, which is similar in design to the One-half 20 transducers, where the HTF diaphragm is at the end of the rigid stainless tubing at the bottom left of the figure. The capillary within the device transmits a pressure wave through the length of the stainless steel tubing where the electronics unit is shown at the upper left portion of the figure. The Gefran PTs are temperature compensated where the thermocouple connection at the lower right of the figure is for this purpose. The temperature is measured is at the tip of the transducer and the remainder of the transducer, including the capillary, is not temperature compensated or temperature controlled. The Gefran transducers have an upper temperature limit of 535 °C which is due to the strength reduction of the PH15-5 stainless steel used in the threaded portion of the transducer end as well as temperature limitations of the diaphragm. Because this is a potential safety and performance issue, there has been no approval to take these sensors above 535 °C. Gefran has developed a pressure transducer that may be an improvement over this type by changing the thread to a larger thread size and employment more thermally robust materials for construction.

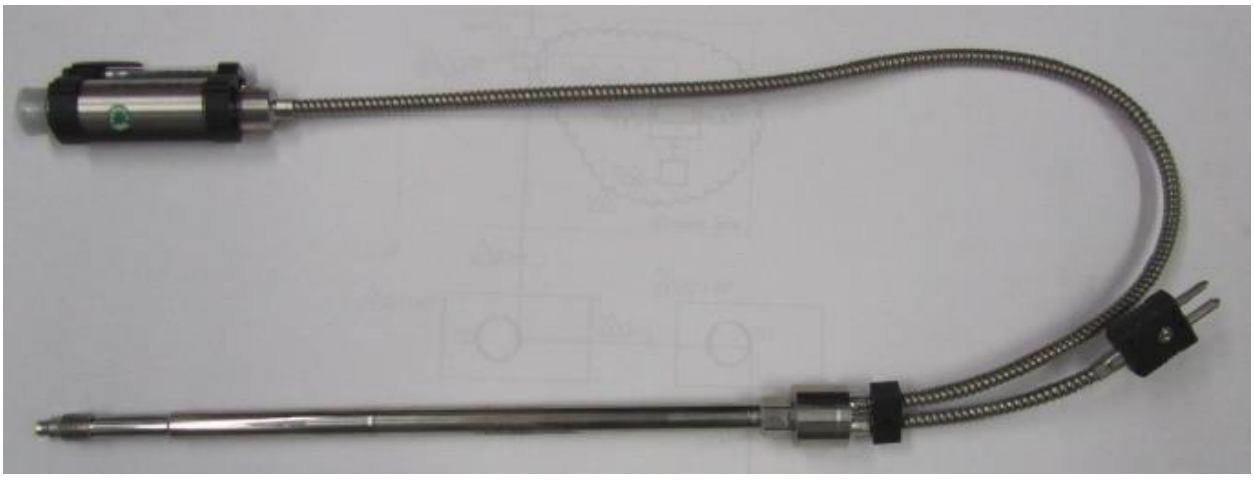

Figure 6. MSTL Gefran Pressure Transducer [36].

2.3.4 Flow Measurements

The flowmeters utilized in MSTL are double-pass, ultrasonic flow meters manufactured by Krohne. These flowmeters are installed on each of the 3 test loops in the MSTL system. The performance of these flowmeters has been tested by using the pump speed to determine the expected flow from a respective pump curve [36]. The pump curve is derived from measured data in a water test at ambient conditions and then scaled for molten nitrate salt's specific gravity and for temperature. Also, a test was performed in which the pump was run at a constant speed, the backpressure control valve put at a specific position, with 400 gpm flow through each test leg. Though imperfect in testing due to differences in pipe length, this test showed the flowmeters to agree under flow control with pump speed matching within 6%. Some mismatch in pump speed is expected because the flow paths to test loops 1 and 3 differ by approximately 80ft. An additional potential error source in this test is the valves which could have slightly

different limits positions and a 0.5% measurement resolution in the valve position. Throughout the operation of MSTL, the flow meters have not appeared to exhibit noticeable drift, their output appears to be very consistent meter to meter where the flow measurement appears to be accurate [36]. However, these flowmeters have a temperature limit in the technical specifications of 535°C [37]. For operation of MSTL, SNL was given a special guarantee that the meters would perform accurately and safely up to the maximum design temperature of MSTL of 585 °C. So, while these meters were acceptable for this application, they likely would not be acceptable for a CSP plant that had to meet production guarantees. These flowmeters are not capable of meeting the >650 °C where further research into higher temperature flow meters for higher-temperature molten salts (e.g. Chlorides, fluorides and carbonates) are being proposed. The limitations for the current meters is not clear as it is likely due to the material challenges at temperatures above 600 °C where stainless steels lose much of its strength and the materials of choice are high temperature nickel superalloys. It may be difficult, or at least expensive to provide flowmeters with these materials. For some applications, the desired material properties seem to be difficult to achieve with nickel superalloys, which also include manufacturing challenges due to their work-hardening tendencies. Additionally, few electronics devices will operate at these temperatures, requiring remote mounting. This requires the use of temperature controlled dead-legs or intermediate fluids in the transducer to remove the electronics to a cooler area. An outstanding observation was that the MSTL flow meters required no insulation be placed around them. So in contrast to the rest of the piping, valves, furnace, and MSTL equipment which is heavily insulated, the flow meters are open to atmosphere. The meters must still be heat traced to prevent salt freezing in the main flow path and therefore the flow meters consume considerable amounts of energy when the system is not flowing salt. This point is illustrated by Figure 7, which shows the piping with only half of its insulation thickness installed.

Figure 7. Flowmeter in MSTL, which remains uninsulated [36].

An initial Failure Mode and Effects Analysis (FMEA) was performed for MSTL, where the loss of flow measurement was determined to be a severe failure mode because of the need to determine quickly and accurately if there is a breach in a customer's test. With the improved performance of the pressure transducers, a test was performed to determine if the pressure transducers could measure the flow on both sides of a valve to accurately determine flowrate. The use of a pressure drop to measure flow is a very common practice, though it is usually done with a device having a single flow coefficient, C_v, such as a knife-edge orifice plate or a Venturi. Because these devices have not been successful in salt applications (due primarily to poor pressure measurement) there is not an orifice or Venturi flow meter installed in the MSTL system. Without this fixed- C_v component, a characterized variable C_v device is the next best choice and the valves were provided with C_v curves at different valve positions. A test was run in which a broad set of flow and pressure conditions were evaluated with the pressure drop measured across Flow Control Valves 1 and 4 (FCV-1 and FCV-4). FCV-1 is used to set the flow and an initial pressure drop within test loop 1 [36]. FCV-4 is used to set the back pressure of the entire system. Both of these valves have pressure transducers on both the upstream and downstream sides of the valve. The nominal test conditions are shown in Table 5 where the results of the test are shown in Figure 8, which show that valve 4 gives reasonable results around 100 psi operating pressure (Tests 4 and 8) but the flow values get worse with increasing system pressure. The tests results indicate that it will not be possible to rely on the valves and pressure transducers as a corroborating flow measurement, and so another method is required, especially above 535 °C where the pressure transducers are not rated for operation [36].

Table 5. Test Conditions for the Pressure Sensor / Flow Meter Evaluation [36].

Test Number	Pressure (psig)	Flow (gpm)	Pump Speed (RPM)
1	200	400	1130
2	300	400	1321
3	400	400	1489
4	100	500	1065
5	200	500	1237
6	300	500	1401
7	400	500	1536
8	100	500	1037
9	100	600	1187
10	200	600	1355
11	300	600	1488
12	400	600	1604

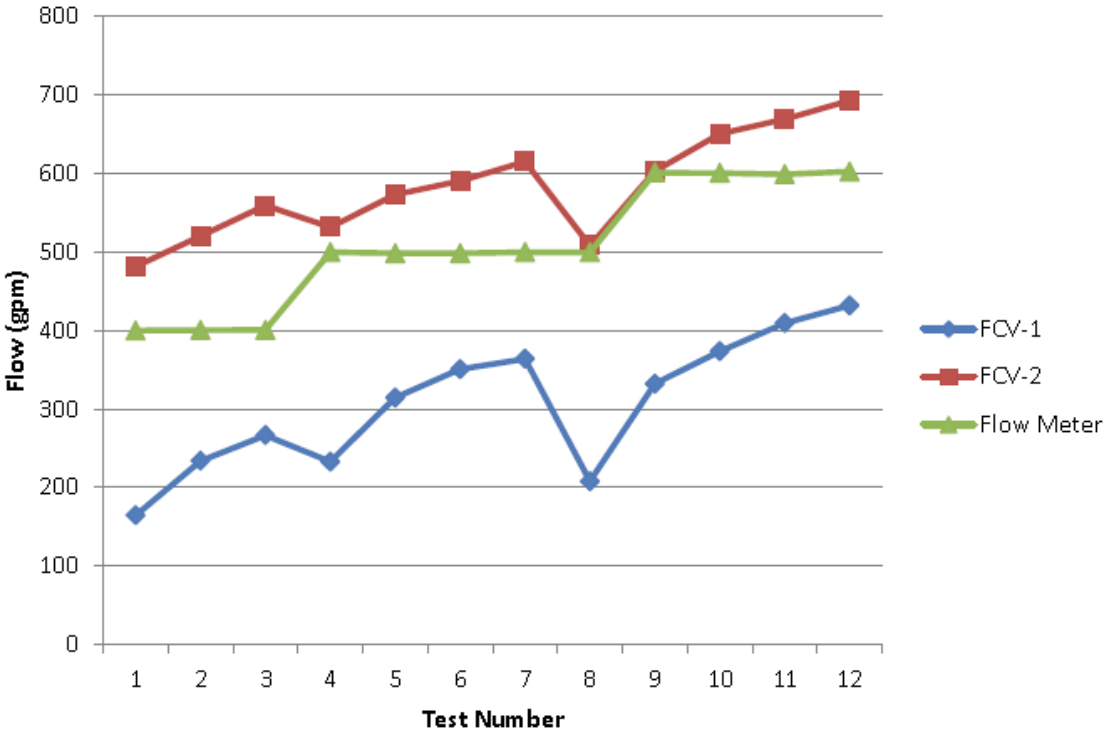

Figure 8. Flow results from flowmeter and pressure drop test showing poor agreement between the pressure Drop and Flow Meter [36].

2.3.5 Mechanical Interface

MSTL provides 3 connection points for the parallel testing of 3 customer's experiments as shown Figure 9. The inverted U-bend is removed and the customer's experiment is attached at that point. The experimenter shall mechanically connect to the MSTL system through 6" nominal diameter pipe of appropriate schedule to withstand the test rig pressure capability with temperature derating and test lifetime considerations. The experimenter's apparatus will typically be welded to the pipe, though high-temperature flanged connections may be considered for shorter term experiments or experiments that need to be disconnected from the system on occasion (as determined by the MSTL engineer).

Figure 9. The customer connection point for loop 1 [36].

Testing with the capillary with added insulation, Figure 10 showed that the heat from the pipe and salt system had a significant effect on the measured pressure values. The salt flowing in the pipe heated the capillary and caused a large increase in the reported pressure. Additionally, even with the capillary insulated, the diurnal temperature swing caused a matching pressure change.

Figure 10. Test Performed by Wrapping the Box Containing the Electronics with Insulation [36].

This result indicated that insulating the capillary was not sufficient and that the electronics package would have to be fully insulated as well. In addition, it was apparent that the capillary and electronics package would have to be heated to such an extent that the pressure transducer would maintain a constant temperature whether salt was flowing or not. To test this theory, an electronic junction box was attached to the end of the pressure transducer protection pipe and the entire capillary and electronics package were placed in a protective box which was insulated externally, Figure 11.

Figure 11. The Capillary and Electronics Package Were Placed in a Box with a Heater (seen at the bottom of the box) [36].

A heater was placed at the bottom of the box as can be seen with a flat metal strip with terminal posts. The results of this test were positive, thus providing a more permanent solution, where a box-in-a-box concept was developed as shown in Figure 12. Here, the inner electrical box is connected to the pipe that protects the pressure transducer. This inner box contains the capillary, electronics package, and a PID controlled heater. This inner box in surrounded by a larger outer box which has a 2 in. spacing for insulation all around the inner box.

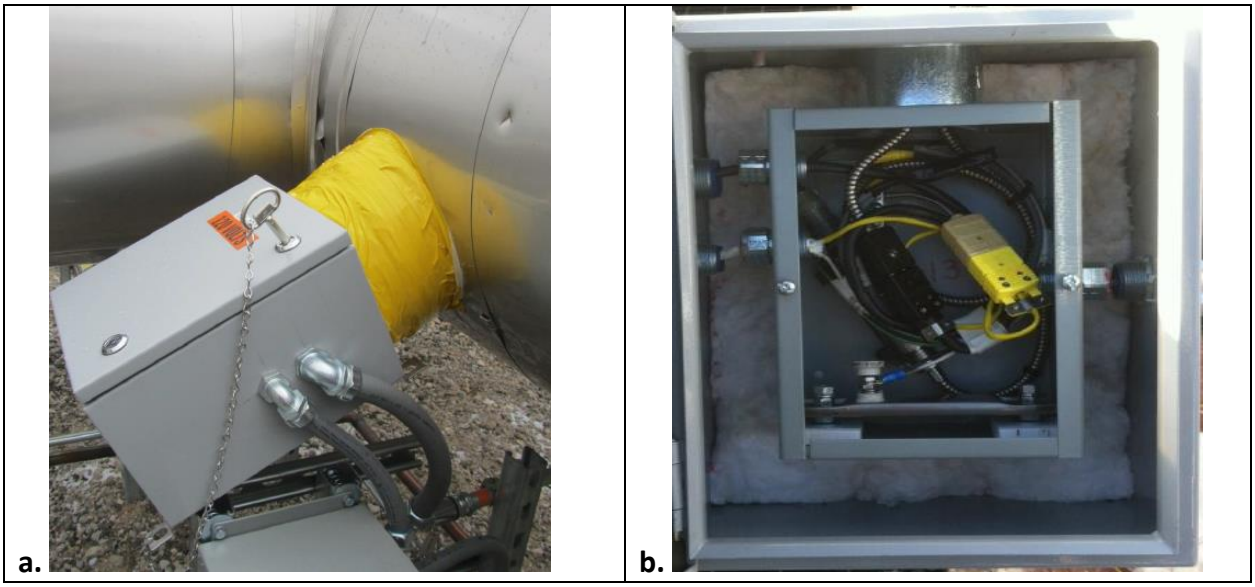

Figure 12. The Completed Box-In-A-Box Concept with Temporary Lagging on the Pipe [36].

In Figure 12b, the insulation can be seen behind the inner box, but the insulation has not yet been added to the sides and in-front of the inner box. This configuration has significantly improved the pressure transducer performance over previous configurations. The stability test results over a 22 hr. period found that the 190psig pressure swing of previous tests was now reduced to 20 psi or less [36]. Additionally, the pressure transducers did not experience a large drop-off in reading after the heat of the flowing salt stops at noon.

Flanges that have been employed are Grayloc brand 6” hubs with silver coated seal rings. The material of the experiment must typically be 300 series stainless steel, Inconel 625, or Haynes 230. The MSTL piping is currently SS347H, so welding to the system is most easily done with 300 series stainless. Other materials will be considered on a case-by-case basis by the MSTL engineer depending on system configuration, the salts employed and other experiments currently in the system. The pipe location for each experiment is listed in Table 6. The surface of the test area is gravel, so the exact height to the pipes can be adjusted slightly, though the preferred method would be to have the experiment raised to the specified height. During power loss, the system uses gravity for drain back, requiring a vacuum relief valve at the highest point. If drain-back from an experiment is not possible, then the experimenter must either be willing to have their experiment freeze-up or must have some other means of addressing salt flow and phase change in a power-off condition.

Table 6. Experiment connection and test area dimensions [36].

Test Stand	Pipe Height	Pipe Size	Pipe Connection	Available Test Area
1	6’	6” sch80XP	Butt Weld	35’x67’
2	6’	6” sch80XP	Butt Weld	30’x67’
3	3’	6” sch80XP	Butt Weld	25’x67’

The MSTL system is designed to have stationary inputs to the experiment that do not transmit force, torque, or expansion. Therefore, there must be accommodation for all thermal expansion within the experiment through the use of sliding mounts, flexible couplings, or other means to minimize the stress and motion that is put on the MSTL system to prevent stress failure from pipe bending. Determination of the minimized stress and motion allowed must be approved by the MSTL engineer.

2.3.6 MSTL Test Application

With significant input from SNL researchers, AREVA Solar designed a 100-foot-tall A-frame structure and Compact Linear Fresnel Reflectors, Figure 13, which are mirrors arranged in rows at ground level. The goal was to explore different technologies to collect and store heat generated by the reflectors in molten salt. Goals were also to demonstrate the viability and performance of a Linear Fresnel system that uses molten salt as a working fluid, thus providing steam at higher temperatures (up to 585 °C) while delivering a cost-competitive storage solution for CSP projects. Compact Linear Fresnel Reflectors are attractive because they can generate a large amount of heat cost-effectively, using a comparatively small land area. The mirrors were aligned to focus the sun’s reflected light at the top of the structure as the heat input, which housed stainless steel receiver tubes through which the molten salt was pumped and then returned to a hot tank of salt, which was used later to produce electricity.

Figure 13. AREVA MSTL application using Linear Fresnel lens mirrors [39].

2.3.7 MSTL Current Status, Restart Path Forward, and Facility Customers

As of September 2017, MSTL has not been used for over two years; the system is currently off-line and some salt freezing has occurred; the MSTL still has the nitrate salt from the last experiment. Despite some weathering, the degree of *exterior* disrepair appears minimal, and is due in large part to Albuquerque's arid climate; refer to Appendix A for a comprehensive set of pictures that were taken of the MSTL on September 2017. More comprehensive inspections of the MSTL show that it requires maintenance to become operational again, including re-melting the existing solar salt inventory. In addition, there are sub-components that would require significant effort to become operational, including valves and pumps. The approximate overall cost for this startup ranges from $500k to $1M.

Generally, there remains a significant need to develop both pressure and flow metering equipment that will be usable in temperatures over 535 °C. This is required to achieve higher temperatures with sensible molten salt heat transfer and storage materials, such as chloride and fluoride molten salts. However, prior research [40] has shown that operation with nitrate salts may develop a protective oxide layer that can further impede corrosion, thus allowing for potential operation with chloride or fluoride salts.

The piping contained in MSTL is currently composed of SS 347. It is strongly recommended to upgrade to nickel-based alloys, such as Inconel 617 or Haynes 230 alloys for piping and component construction. These materials could provide more reliable performance in comparison to stainless steel alloys for chlorides and fluorides in the areas of corrosion resistance and mechanical strength. To ensure the pumping system in MSTL was able to operate under the presence of more corrosive salts than nitrates, it is strongly recommended that electromagnetic pumps (EM) be employed to facilitate flow for chloride and fluoride molten salts [41].

The $500k to $1M startup cost estimate is based on a meeting held on September 18, 2017, with the purpose of seeking pathways to restart the facility. The attendees included Charles Andraka, Ronald Briggs, Kenneth Armijo, Richard Sisson, and Sal Rodriguez. During the meeting, it was noted that MSTL has five variable flow valves, each valued at $80,000. The valves are full of solid salt, and will need repairs, including replacement of gaskets and various internal components. The pump (which cost $1 million), will also need some repairs, while the solidified salt in the tank will need to be melted at a slow rate to avoid damage to the salt (overheating), as well as stresses on the loop components. Thus, under an optimistic scenario, the estimated cost is $500k, while under a conservative scenario, all the valves will need replacement, thus reaching a cost of about $1M. However, the cost to build a new plant (if an acceptable design plan existed), would cost about $10M for parts and assembly. Thus, MSTL restart is more cost-effective than building a new facility.

During the meeting, it was noted that the Nuclear Science User Facilities (NSUF) has expressed interest in restarting MSTL, and wants to include it as a user facility. In addition, MSR-TWG has expressed a strong interest in using MSTL and/or collaboration regarding salt loop operation and design. MSR-TWG will meet with SNL personnel on October 2, 2017, for a closed-doors meeting to seek a path forward, including GAIN proposals. In addition, SNL personnel will present MSTL

capabilities and unique SNL technical capabilities at the Molten Salt Reactor Workshop at ORNL on October 3-4, 2017.

Finally, it was agreed that a slow heat-up rate would be the most benign approach for restart, and that flushing of the nitrate salt was important, especially if other salts such as fluoride or chloride are used in the loop. If the loop material composition is not replaced with a higher-temperature alloy, then the loop maximum operating temperature will be constrained by the SS 347 piping. It was also suggested during the meeting that the loop could be sectioned, so various salts could be tested. Another potential use made by SNL's safeguards group is to add fission surrogates onto the molten salt mixture.

2.3.7 Recommended Research Activities for High-Temperature Fluoride Salts

Research for fluoride molten salt reactors could take place within a two-pronged intrinsic/extrinsic process where both fundamental sciences would address thermodynamic phenomenological challenges that exist with fluoride salts, particularly with various materials that would be contained within the present MSTL system, and for scoping which materials could be used to replace potentially problematic components.

2.3.7.1 Intrinsic Studies

Research would first investigate and publish thermophysical properties for heat capacity, viscosity, density, thermal stability, and thermal conductivity for the candidate salt compositions across the range of planned operating temperature range up to 750 °C for static tests. These tests may include the salt pots for understanding reactivity, kinetics and determine impurity effects on properties from industrial-grade salts. Here, additional work could be conducted with fluoride salts, containing both binary and ternary components to determine if product mixtures could have better characteristics with respect to cost, melting point, heat capacity, material stability, and corrosivity. Here, one would optimize salt composition with the goal of minimizing corrosion with both static and dynamic component material reactivity. Researchers could specify baseline melting and purification protocols for commercial salts, ullage gas composition, and any other process requirements (fluoride and chloride-based salts). Additionally, this fundamental research with fluorides will be performed to investigate their kinetics, material stability and performance for applications within a molten salt loop. Here, three alloys/materials would be immersed in a fluoride salt at 700°C for 500 hours, similar to research performed at the NSTTF [Kruizenga paper]. Materials would be chosen based on expected piping and wetted surfaces for rotary joints in the system. This work would also be used to demonstrate freeze recovery with high-melting salts to determine importance of melting point.

Following exposure in the molten salt, corrosion allowances will be estimated using ASTM codes and standards methods, with provided results by design engineers. Limited optical microscopy will be performed to assess any morphological changes on the surface of the alloys. Tests will be performed by slowly sparging the salt/alloy with an inert gas throughout the duration of the test. The purpose of this sparge is to test the feasibility of employing industrial sparge gasses to avoid the formation of oxohalides, which appear to exacerbate corrosion in molten fluoride systems.

2.3.7.2 Extrinsic Studies

Engineering design work during this phase will address materials, thermo-fluid reliability and temperature constraints, for components that will reside within the skid-mounted system. Here, initial assessment for the MSTL facility would be conducted to evaluate potential employment for the current piping and flow components, instrumentation and controls, to evaluate reliable operation using fluoride salts. Modular designs may be considered with separate dump tanks for testing with multiple types of salts within the three separate loops. Depending on the composition, integrated heaters and heat trace will have to be installed appropriately to operate against molten salt freezing conditions. A materials compatibility investigation will be conducted to determine selection based on respective system temperatures, pressures, flow rates/stress and chemical kinetics. For this work, Low-Ni concentration 600 series stainless steel alloys or Inconel 617 will be considered for heat rejection boilers and storage tank containment reservoirs. These alloys, in addition to Hanyes 230 will also be considered for added piping and control valves. This work will also include advanced design work of high-temperature molten salt system connections to account for leaks that are prevalent within flanges and joints [40] due to their incredible wetting properties. Currently, welded joints are employed as a solution to address molten salt leakage as the result of thermal expansion of bolts within flange joints. However, welded joint connections can be expensive and time-consuming for installation as well as operation and maintenance (O&M). For this work, non-welded connection designs may be investigated to assess novel mechanical seals and flange connections. Here, this investigation could then explore the development of advanced tapered mechanical clamps that will be well-insulated and heated to address flange expansion/contraction issues.

For reliability, accelerated movement tests will first be conducted for the pumps, valves and heating subsystems to assess their durability under high-temperature conditions in order to withstand thousands of cycles without salts. Next, accelerated lifetime and heat aging tests will be performed with molten salts to ensure 0% leakage rates from all connections and welded joints. For these tests the loop will be operated for 1440 hours (about two months) to assess component/system durability. Here, rigorous corrosion and thermal experimental analysis of the collector and system will develop a fundamental understanding of collector and system performance and mitigate reliability risks.

This novel capability will be a valuable addition to SNL National Laboratory CSP resources. The model validation work would leverage SNL NSTTF thermal-fluid modelling platforms where fundamental research performed in Phase I related specifically to chloride molten salt will be incorporated for optimization design modelling of the test loop. These scalable prediction models will be related to multiphase thermal-hydrodynamics transport, corrosion, and optical efficiency.

3. MSR Safety

The NRC is currently assessing their need for MSR modeling capabilities, and MELCOR – actively maintained and developed at SNL – would be a prime candidate for the requisite safety and

accident analyses. The Office of New Reactors (NRO) has simultaneously tasked SNL to conduct a simplified scoping assessment of radionuclide releases from advanced reactors including MSRs.

MELCOR is well-established as an analysis tool for Light Water Reactors (LWRs), but recent code development efforts have endeavored to expand modeling capabilities into the "non-LWR" category with attention to Generation-IV reactor technologies. The NRC recently requested a status update on MELCOR and its non-LWR modeling capabilities, including an assessment of its readiness to handle several MSR design concepts being pursued with varying levels of interest by the nuclear industry. A typical concept for an MSR is shown in Figure 14. There are no MELCOR models that target MSRs specifically, but to that end there are 1) existing models that could be augmented/expanded and leveraged, and 2) new models/capabilities that could be added. The following is a general outline of as-yet identified competencies and shortcomings with respect to MSR modeling in MELCOR. Issues related to both broad categories of MSR design (solid-fuel and fluid-fuel) are discussed first, and special concerns associated with each category are discussed thereafter.

Whether the MSR design in question is solid-fueled (as in typical LWRs) or fluid-fueled (where fuel and coolant salts flow together in the primary loop), MELCOR must be able to model equation-of-state and thermophysical properties for generalized molten salts. One outstanding question is whether the general working fluid read-in utility (developed for sodium fast reactor modeling) is adequate for this purpose, and whether it could handle salts in both the molten and frozen states. Since SNL has access to molten salt property data, a test problem could easily be created and performed in relatively short order. Another potential issue has to do with the capability to model two or more different working fluids (that may or may not be condensable) with the Control Volume Hydrodynamics (CVH) physics package in the same problem. There could be a need for such a capability, particularly if multiple salts are to be modeled or if the secondary power-production side of an MSR must be modeled. That is, there may be a super-critical water, Rankine, or Brayton power cycle coupled onto the MSR. Existing MELCOR capabilities for heat exchanger and pump modeling are likely adequate (or can readily be made so) for MSR purposes. Additionally, new chemistry models will need to be incorporated. Existing MELCOR chemistry models could serve as blue-prints for constructing new molten salt chemistry models.

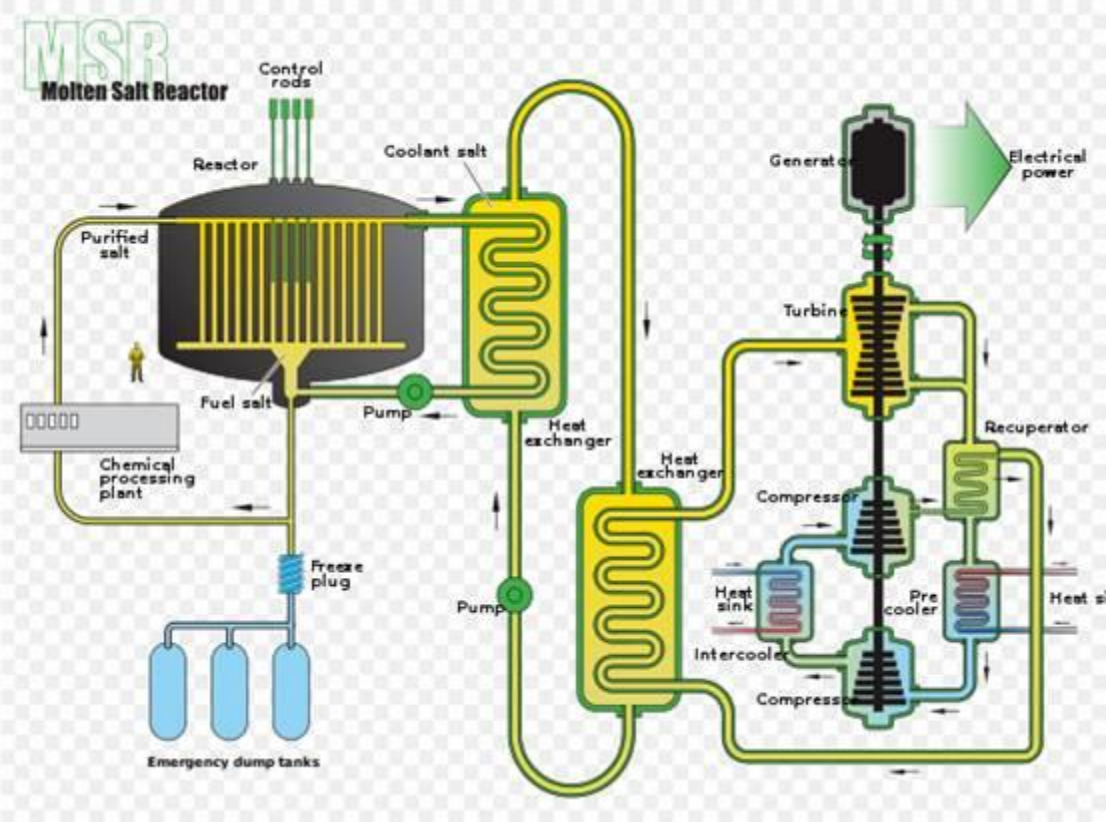

Figure 14. Typical MSR design configuration.

With regard to solid-fuel systems, MELCOR in its current state is in a better position to handle core modeling in the context of both normal operations and severe accident conditions. The fixed core fits within the MELCOR core (COR) physics package paradigm (two-dimensional, azimuthally-symmetric cylindrical geometry consisting of a complex of "rings" and "levels"). Furthermore, prior work on High Temperature Gas-Cooled Reactors (HTGRs) led to new MELCOR models for pebble-bed and prismatic-type TRISO-fueled cores related to heat transfer, fuel failure, fission product release, etc. Since some solid-fueled MSRs use fuel elements similar to those of HTGRs, these newer HTGR MELCOR models could be utilized as-is or after slight modifications to account for fuel geometry and other effects. There are other concerns that should be identified via some sort of Phenomena Identification and Ranking Table (PIRT) process. In general, these issues would be related to in-vessel and ex-vessel phenomena that bear relevance to source term calculations.

Fluid-fuel systems represent a large departure from MELCOR COR package modeling assumptions of a fixed, structural reactor core. It is unclear if the COR package must be drastically augmented (a new reactor type with new physics models) or if the fluid-fuel modeling issue could be finessed through use of the CVH package and user-supplied enthalpy sources that reflect fission power and decay heat addition. There is a litany of new phenomena to consider with this MSR design, and development efforts would benefit from a PIRT study. To name a few issues:

- Reactor kinetics considerations (delayed neutron fraction model, new feedback effects related to fluid fuel density and fluid fuel flow rate into the active core region).
- What does it mean to model "failure" of a fluid fuel?
- Can fluid-fuel fission product transport be modeled?
- Can fluid-fuel clean-up systems be modeled?
- Are new ex-vessel models needed (e.g., for freeze-plugs and drainage tanks)?

While these tools are being developed, SNL will need to develop approaches to estimate site boundary doses for MSR accident sequences. The current approach will be to conduct a leak-path factor analysis on assumed releases from the MSR. ORNL has offered to host a SNL research team to discuss the release barrier safety analysis approach conducted by ORNL for the original Molten Salt Reactor Experiment and transfer all relevant documentation to SNL.

4. MSR Safeguards

SNL will begin an effort in FY18 to develop a safeguards performance model for MSRs as part of the Material Protection Accounting and Control Technologies (MPACT) program at DOE NE. The program supports safeguards and security work for the fuel cycle, and one of the program goals is to help support the DOE NE mission.

The recent interest in MSRs is leading to renewed interest in the challenges of safeguards associated MSR designs. In particular, liquid-fueled MSRs require an on-line processing capability to remove fission products and add new fuel or fissile material periodically. Designs may include continuous on-line processing or reprocessing at select times. Liquid fueled reactors have many safeguards challenges since materials accountancy moves from item accounting to bulk processing systems, which require safeguards measurements similar to reprocessing plants. For this reason, only liquid-fueled designs will be considered for safeguards modeling. (Solid fueled designs have safeguards requirements similar to light water reactors.)

The MPACT project will use the existing Separations and Safeguards Performance Model architecture in Matlab Simulink to develop a safeguards model for MSRs. Past work has developed safeguards models for pyroprocessing plants, which also use molten salt, so many of the functions are directly applicable. The key difference is that depletion will need to be added to the model by linking to ORIGEN. Figure 15 shows an example of an existing pyroprocessing model. The model tracks elemental and isotopic material flow through the various unit operations, and simulates measurements required for safeguards. The safeguards system is the focus of the model and includes calculations for material balances, error propagation, and statistical tests.

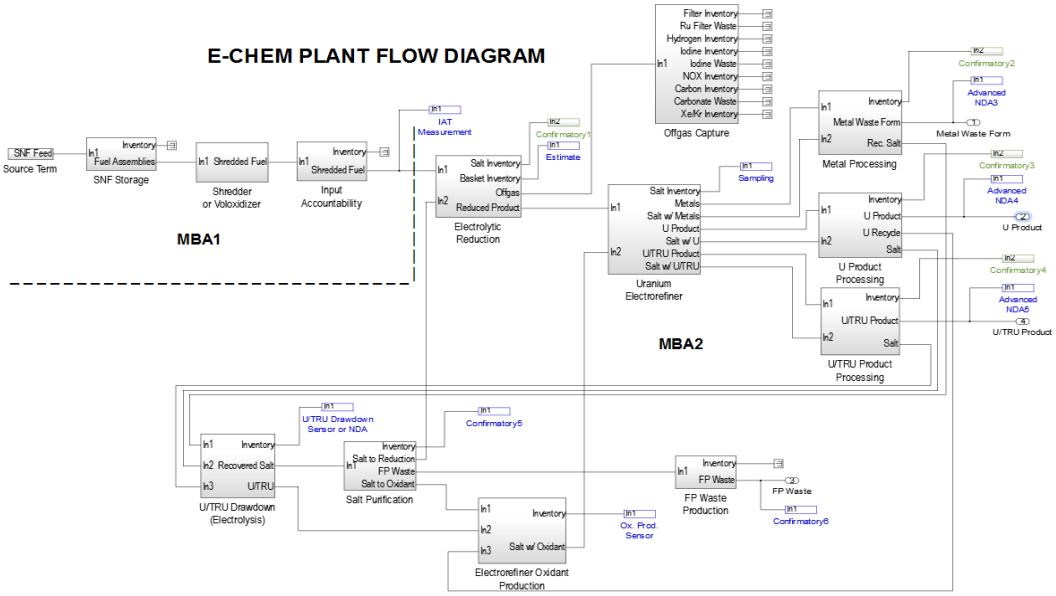

Figure 15. Example Safeguards Model for Pyroprocessing.

The work will use a generic design for a liquid-fueled MSR. The goal is to set up the model so that it can be easily modified to represent different fuels, size, and reprocessing timing options. The integration with ORIGEN will likely require Matlab to call ORIGEN periodically to update source terms. This integration can be rough since the main focus of the work will be on the safeguards system.

SNL's goal is to develop a MSR safeguards model within two years, and provide preliminary analyses. Existing measurement technologies (as being tested for pyroprocessing) will be used to determine how well the design can meet regulatory requirements.

The safeguards models in the past have also been used to explore process monitoring and process control. Future work should consider these needs for MSRs as well. For example, the use of an on-line measurement for actinide content may help the reactor operator with reactivity control and to make re-fueling decisions. These additional process monitoring options should be explored in future work, and may find a role in the Advanced Reactor Technologies program.

A potential future molten salt test loop at SNL should also consider if safeguards measurements can be tested. The challenges here are that typically safeguards measurements would require actinide and fission product materials, which might be difficult experimentally. However, even bulk measurements of salt with surrogates may be helpful from a process monitoring perspective.

Most current research and active endeavors to build an MSR stem from the initial MSR built and run at ORNL, and planned follow-on designs (that never were built) in the 1950s through 1970s. However, while ORNL does have historical knowledge and continuing expertise in this area, the issues facing adoption of molten salt and fuels are not confined to ORNL capabilities; SNL has strengths in materials engineering, neutronics, and severe accident simulation.

Molten salt and fuels have an inherent advantage over sodium-cooled fast reactors in that there is no fire hazard associated with sodium ruptures. However, there remain significant materials issues involving molten salts, including:

- Material effects and lifetime of graphite cores immersed in molten salt.
- Different salt chemistries (Flibe, chlorides) which result in very different neutron spectrums.
- Long-term material degradation (stress corrosion cracking, etc.).

Additionally, more work needs to be done on thermal hydraulics for molten salts, applicable to the large variety of reactor designs being proposed, and corresponding severe accident simulations (e.g., MELCOR). While techniques have been tested for dealing with fission products, and on-line reprocessing, works remains. This includes the separation of U-233 from molten salt, if pursuing a thorium cycle).

Regarding safeguards, the main issues revolve around appropriate diagnostics to fully account for fissile material within a molten salt environment. Much of the fissile material will be in-process, so it becomes difficult to "account", which is the standard approach for the IAEA to verify inventory. It appears that current, on-the-shelf diagnostics for safeguards applied to molten salts will not be sufficient, and it is not clear what developments in diagnostics must be done. In FY17, ORNL was tasked with considering this, but they are focused on just one reactor type. It is therefore likely that the results will be diagnostic recommendations. Therefore, there is a strong likelihood that much work will be required to develop new or enhanced safeguards diagnostics for MSRs. SNL has expertise in neutron multiplicity counting, gamma spectroscopy, and advanced NDA techniques that could be leveraged. Additionally, Unattended Monitoring Systems (UMS) will likely be needed for molten salts and fuels since most material is in-process and flowing, so a continual observation diagnostic would be useful. SNL has expertise in autonomous systems that can be leveraged.

Additionally, SNL maintains a robust group for developing safeguards approaches and technologies including recent strategic planning for NA-241 [Farley and Sternat, 2017]. In particular, there are significant radiation issues if thorium is used as an MSR fuel. The decay of Tl-208 releases intense gamma rays (2.6 MeV) that require enhanced shielding and infrastructure (e.g. hot cells) to manipulate the spent fuel. SNL can use its expertise in handling radioactive materials and nuclear security to address this "hot fuel" issue. The safeguards group continues to be involved in all aspects of safeguards development. Clearly, this is a strong point for garnering more work in the molten salt arena.

5. MSR Computational Fluid Dynamics

As of 2017, SNL has the power of 3,706 teraflops through a massively-parallel infrastructure called the High Performance Computing (HPC) network. Along with state-of-the-art computational fluid dynamics (CFD) codes, SNL can provide very detailed analysis over millions to billions of computational nodes. The models include the state-of-the-art large eddy simulation (LES) dynamic Smagorinsky turbulence model, direct numerical simulation (DNS), and Multiphysics computations that couple CFD with heat transfer and structural dynamics [Rodriguez, 2016].

SNL has conducted recent CFD simulations of advanced reactors. For example, Figure 16 shows the natural circulation pattern in an air-cooled nuclear fuel assembly (left hand side), as well as its temperature distribution (right hand side). Figure 17 shows a forced-convection, water-cooled, nuclear fuel assembly simulation using Multiphysics, where the CFD was coupled with heat transfer and structural dynamics.

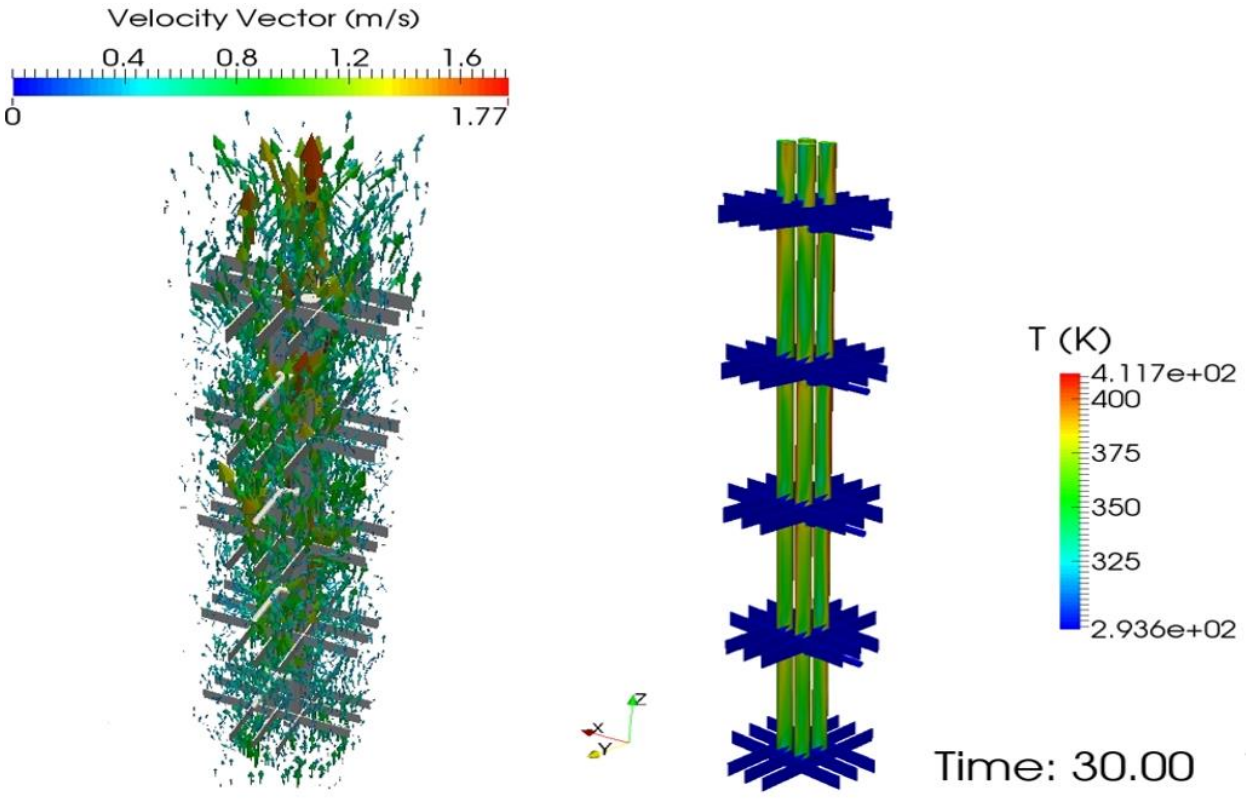

Figure 16. CFD simulation of natural circulation fuel bundle experiment in air—velocity and temperature distribution [Rodriguez, 2016].

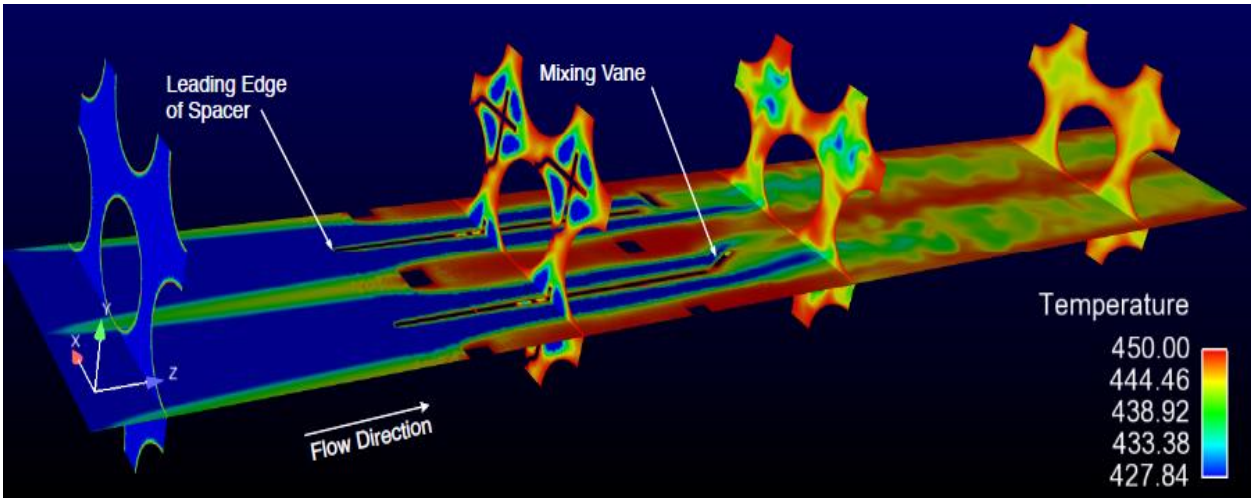

Figure 17. Coupled CFD, heat transfer, and structural analysis of Westinghouse fuel rod [Rodriguez and Turner, 2012].

In the area of molten salt fuel modeling, SNL used CFD to model a cube of molten salt under natural circulation [Rodriguez, 2015]. Because the Molten-Salt Reactor Experiment (MSRE) used LiF-BeF_2-ZrF_4-UF_4 and the Aircraft Reactor Experiment (ARE) used NaF-ZrF_4-UF_4, a fluoride salt with elemental commonality was used. Therefore, FLiNaBe was chosen, and an added benefit is that it is also similar in elemental composition to FLiBe. FLiNaBe physical properties are readily available in the literature [Serrano-Lopez, Fradera, and Cuesta-Lopez, 2013]. The melting point of FLiNaBe is 588 to 611 K, for an average value of 599.5 K. Its density, dynamic viscosity, thermal conductivity, and heat capacity, respectively, are as follows,

(2) $\rho = 2435.9 - 0.45T$ (kg/m^3)

(3) $\mu = 3.38E - 05exp(4738/T)$ (Pa-s)

(4) $k = 0.5$ (W/m-K)

(5) $Cp =$ 2,200 (J/kg-K)

The inlet temperature for this hypothetical molten salt system was $T_{in} = T_{melt} + 100 = 599.5 + 100 = 699.5$ K, while its outlet temperature was $T_{out} = 650$ °C = 923.15 K. For this system, the Prandtl (Pr) number ranged from 25.1 to 130.2, which is significantly larger than that of water. It is noteworthy that most turbulence models are designed for Pr in the range of gases and water, 0.7 to 5. Thus, the ability of CFD models to adequately model molten salts can be of concern. In particular, the high Pr implies that the thermal boundary layer is much smaller than the fluid boundary layer. Consequently, it is necessary that the thermal boundary layer be resolved with a fine mesh at the boundary, typically requiring that $Y^+ < 0.3$.

For the molten salt simulation, the dynamic Smagorinsky turbulence model was used, along with the Boussinesq buoyancy model. The Rayleigh number (Ra) for this model was 5.1×10^9, indicating incipient turbulence. The Nusselt number (Nu) was 171.9, indicating a high degree of cooling from natural circulation. Figure 18 shows the velocity distribution that arises from the natural circulation of FLiBe. As expected, the velocity at the wall is zero due to its no-slip boundary, while the opposite end of the boundary layer remained essentially motionless because the fluid is not heated in that region. Therefore, the velocity distribution peaked about 1/3 into the layer of the boundary layer, as measured from the wall.

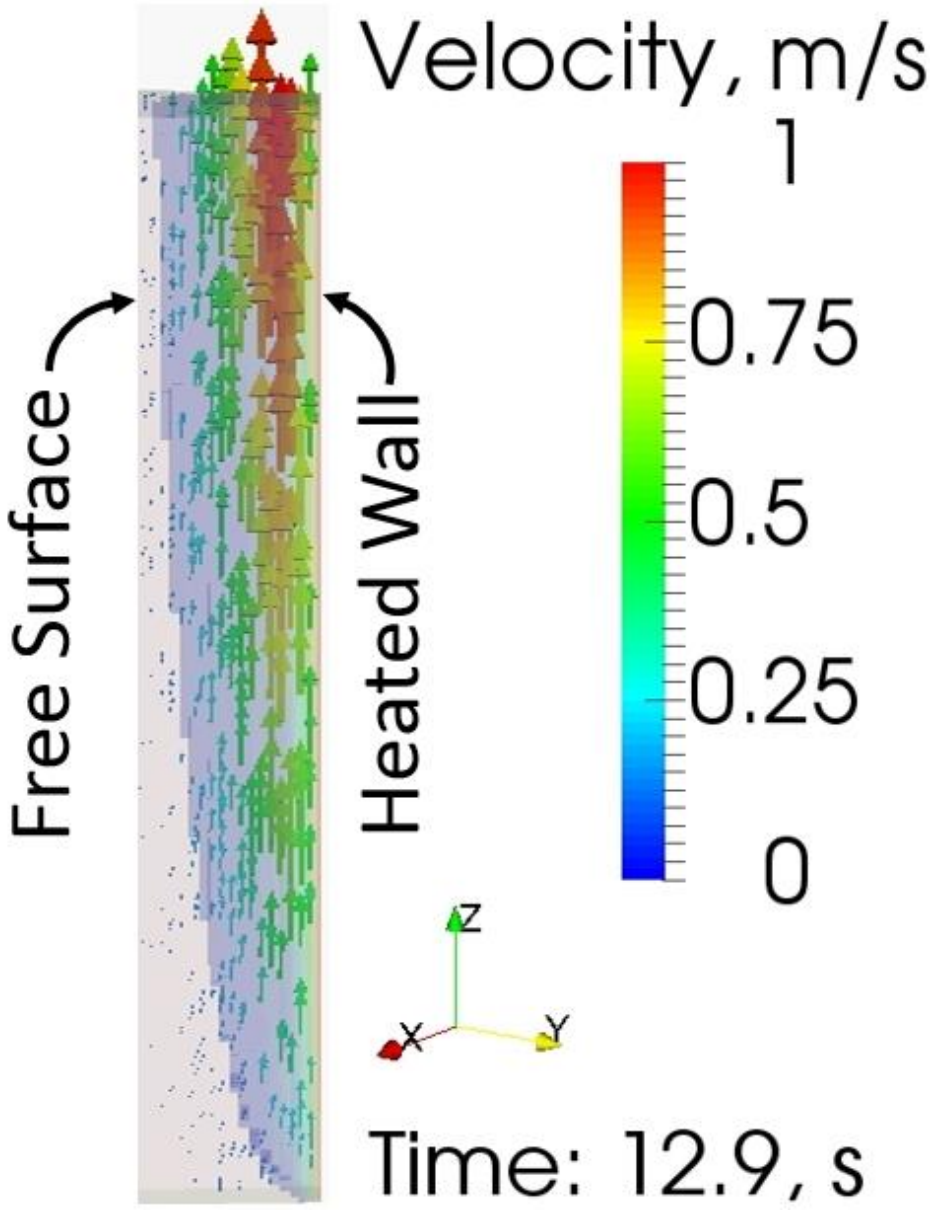

Figure 18. CFD simulation of molten salt under natural circulation under MSR-like conditions

6. MSR Nuclear Criticality Safety and Neutronics

The Sandia Critical Experiments (SCX) facility was designed to perform and analyze critical benchmark experiments for validating reactor physics methods and models. An overall view of the critical assembly at SCX is shown in Figure 19, while Figure 20 shows the operational details of the critical assembly. Figure 21 shows a cut-away view with the internal details of the critical assembly for the 7uPCX configuration. Figure 22 shows the upper part of the critical assembly view. Figures 23 and 24 show the 7uPCX and BUCCX configurations, respectively. Since 2004, SNL has conducted and published seven critical benchmark experiments for the International Criticality Safety Benchmark Evaluation Project (ICSBEP), with plans for additional criticality experiments in the future. In addition, SNL will conduct reactor physics benchmark experiments for the International Reactor Physics Experiment Evaluation Project (IRPhE). Given its versatility and number of successful benchmark experiments, the SCX facility is ideally suited to perform criticality experiments for molten salt based fuels. In addition, SNL's extensive experience in designing, performing, and analyzing critical benchmark experiments are valuable assets for advancing molten salts and fuels at SNL.

SNL has extensive experience in reactor physics and computational methods for neutron transport, with expert users of the Monte Carlo N-Particle (MCNP) transport code. MCNP is a general purpose three dimensional simulation tool that transports different particle types for criticality, shielding, dosimetry, detector response, and many other applications. MCNP, along with the available HPC infrastructure, offer a very powerful tool for simulating the neutronic effects associated with MSRs. For example, Figure 25 shows the MCNP neutron spectrum results for the 7uPCX and BUCCX core configurations at SCX.

Figure 19. Overall view of the critical assembly at the SCX facility.

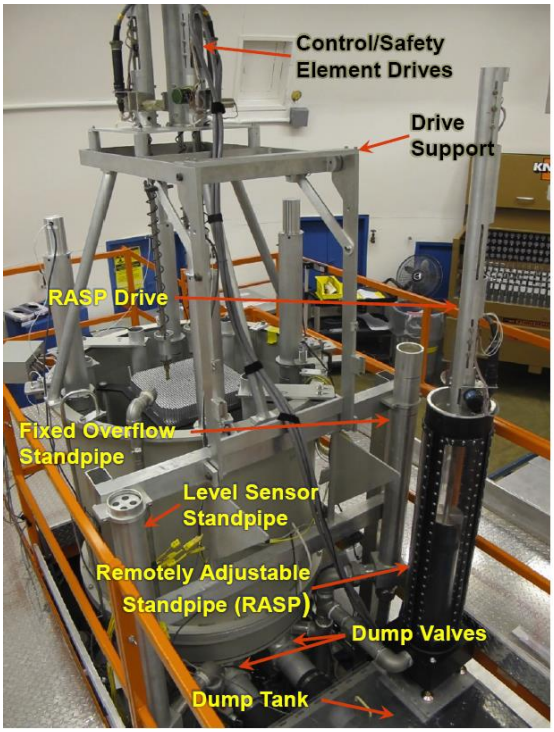

Figure 20. Critical assembly at the SCX facility.

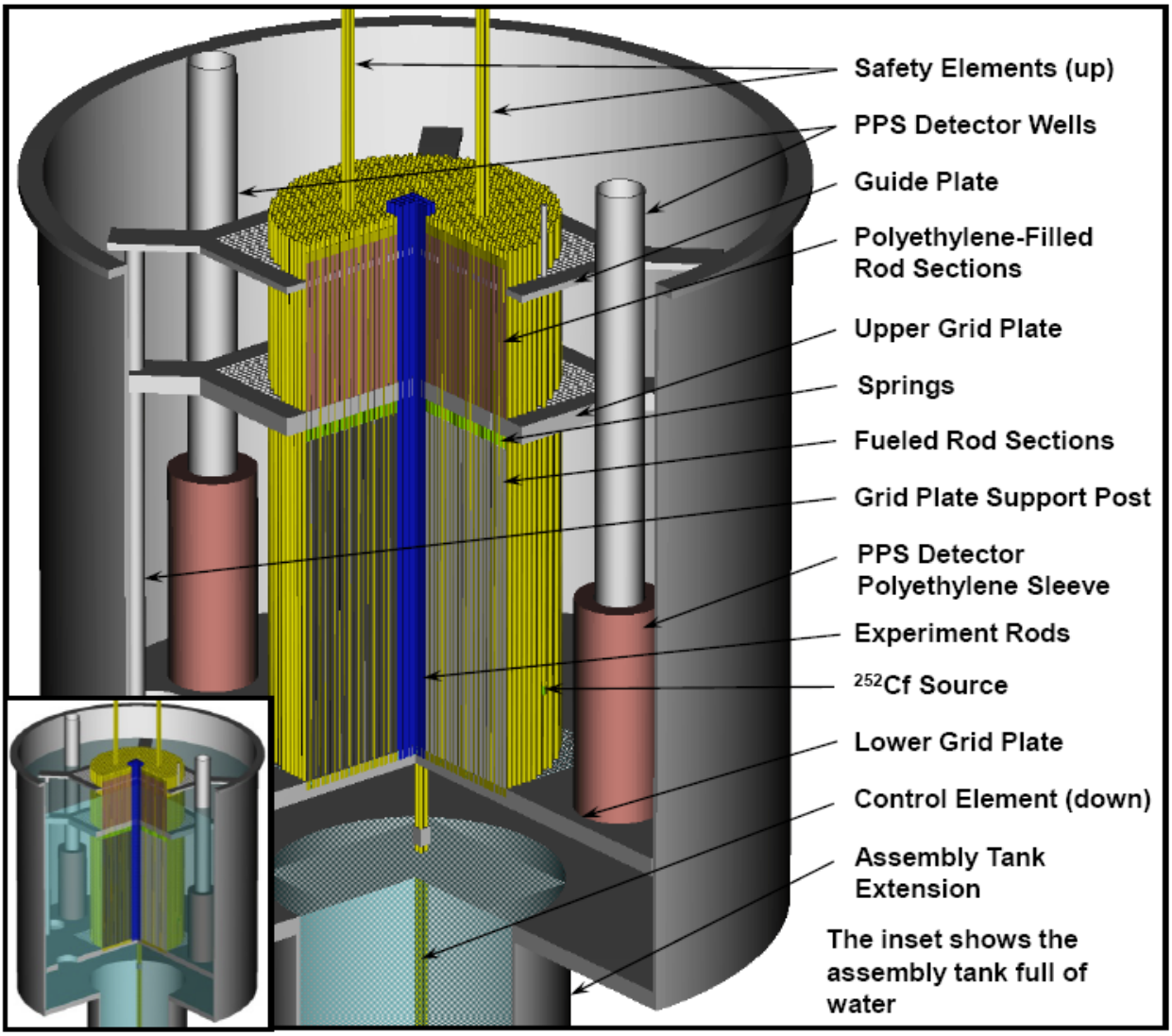

Figure 21. Cut-Away view of the critical assembly (7uPCX configuration).

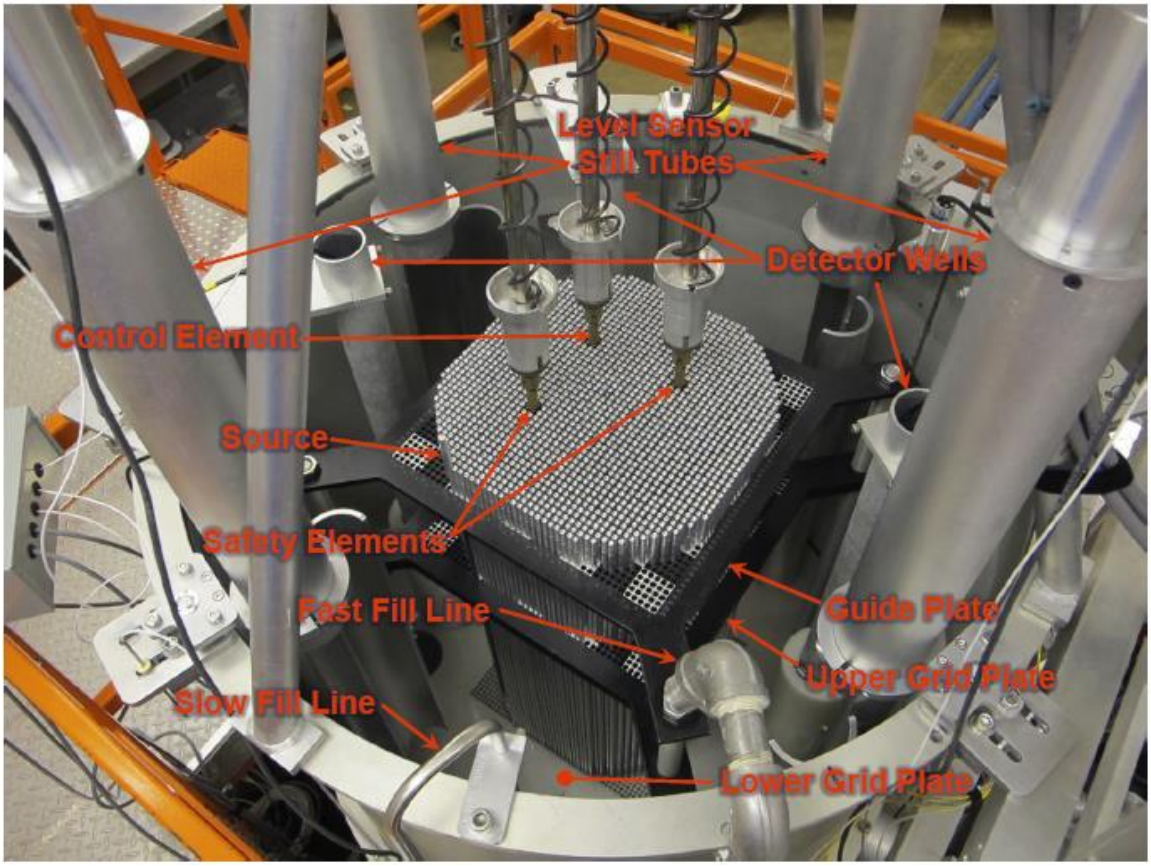

Figure 22. Critical Assembly view (SCX facility).

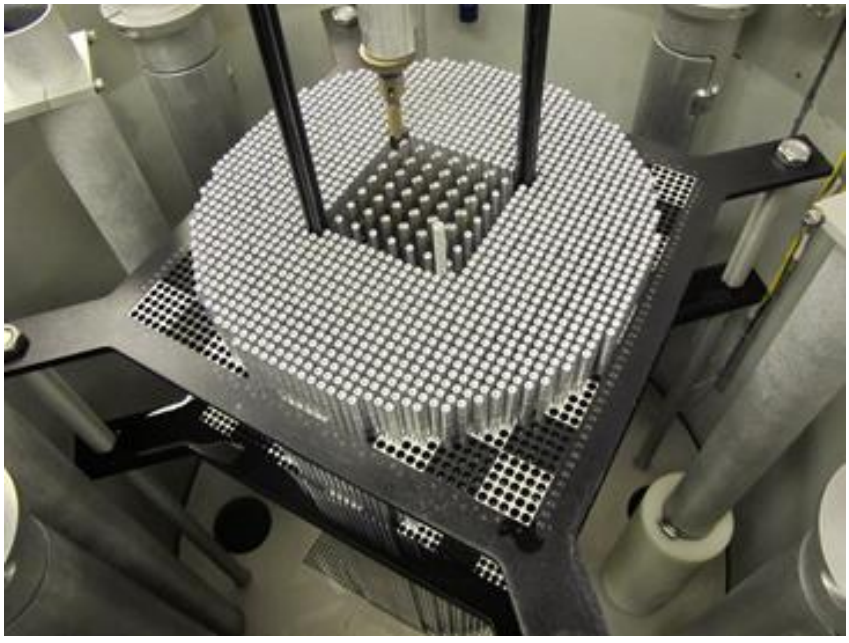

Figure 23. 7uPCX configuration (SCX facility).

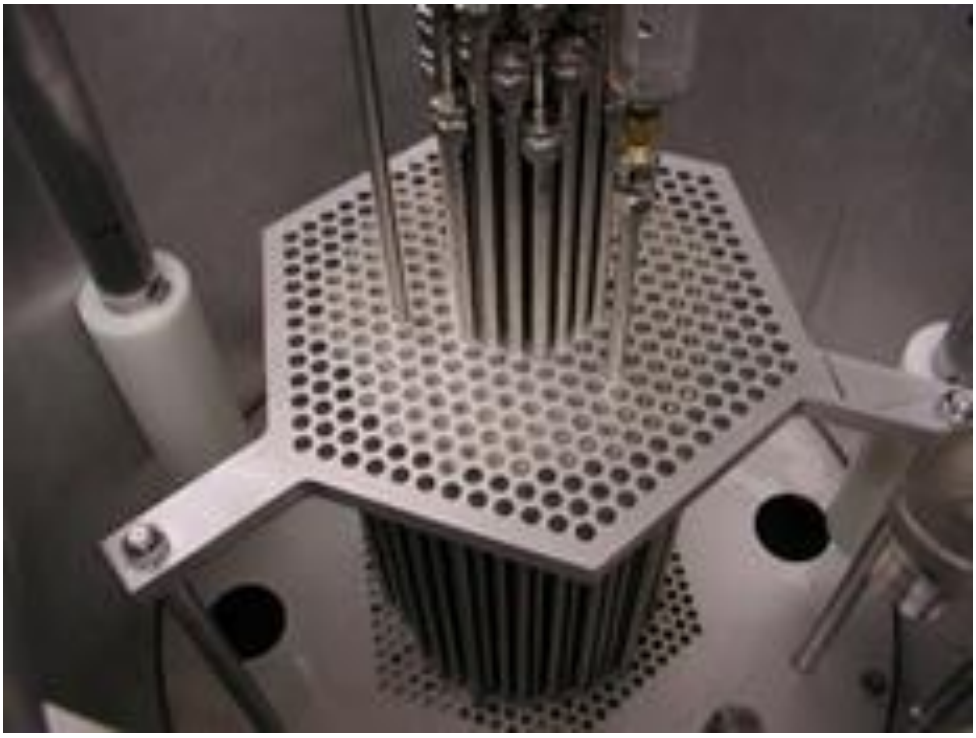

Figure 24. BUCCX configuration (SCX facility).

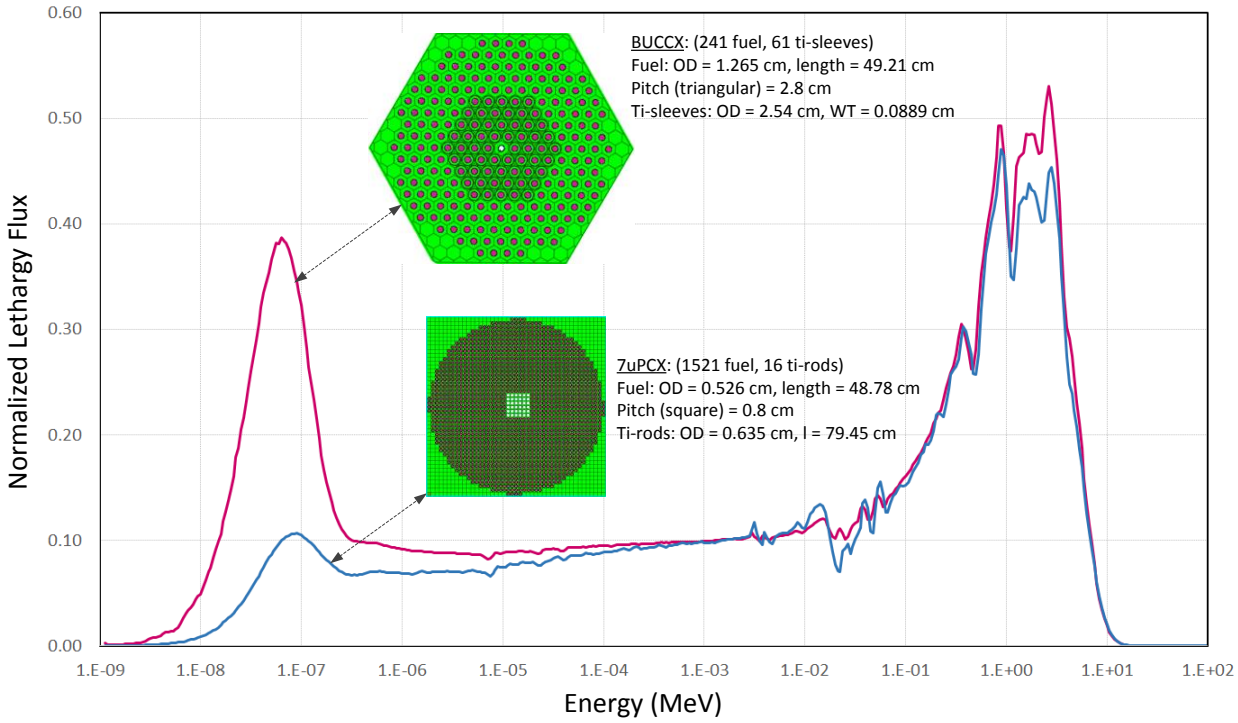

Figure 25. MCNP neutron spectrum results for two different core configurations at SCX.

REFERENCES

Brosseau, D., et al., "Testing of thermocline filler materials and molten-salt heat transfer fluids for thermal energy storage systems in parabolic trough power plants", Transactions of the ASME-N-Journal of Solar Energy Engineering, 127(1), pp. 109-116, 2005.

Bushey, R., "Building the Next Generation of Nuclear Reactors", R&D Magazine, August 17, 2017.

Farley, D. R. and M. R. Sternat, "Strategic Planning for Molten Salt Reactor Safeguards", Sandia National Laboratories, SAND2017-3105, 2016.

Megawatt Workshop, "Safe and Secure Megawatt-Size Nuclear Power Workshop", Washington, DC. https://arpa-e.energy.gov/?q=workshop/safe-and-secure-megawatt-size-nuclear-power-workshop. Accessed on August 25, 2017.

Olivares, R. Chen, C. and Wright, S., "The thermal stability of molten lithium-sodium-potassium carbonate and the influence of additives on the melting point, *J. Sol. Energy Eng*., 134, 2012.

RFI, https://arpa-e-foa.energy.gov/Default.aspx#FoaIdcb9f0638-121e-4f5b-ad37-f53767d3b8bb. Accessed on August 21, 2017.

Rodriguez, S., "CFD Modeling of USU Fuel Bundle Experiment", Sandia National Laboratories, 2016.

Rodriguez, S., "ARPA-E's Energy Strategy", Sandia National Laboratories, August 2017.

Rodriguez, S. and D. Ames, "Design Optimization for Miniature Nuclear Reactors", American Nuclear Society, Winter Meeting, November 2015.

Rodriguez, S. and D. Z. Turner, "Assessment of Existing Sierra/Fuego Capabilities Related to Grid-To-Rod-Fretting (GTRF)", Sandia National Laboratories, SAND2012-0530, 2012.

Serrano-Lopez, R., J. Fradera, and S. Cuesta-Lopez, "Molten Salts Database for Energy Applications", Chemical Engineering & Processing: Process Intensification, 2013.

Stekli, J., "Thermal Energy Storage and the United States Department of Energy's SunShot Initiative," SolarPACES2011, SolarPACES: Granada, Spain, 2011.

Zhao, J. C., "From Giga to Mega: Miniaturize Nuclear Power Plants", ARPA-E Energy Innovation Summit, Washington, DC, February 29 to March 2, 2016.

[1] Pacheco, J.E., Moursund, C., Rogers, D., Wasyluk, D., "Conceptual design of a 100MWe modular molten salt power tower plant," *SolarPACES2011*, Granada, Spain, 2011.

[2] Dunham, M. T., and Iverson, B. D., "High-efficiency thermodynamic power cycles for concentrated solar power systems," *Renewable and Sustainable Energy Reviews*, 30, pp. 758-770, 2014.

[3] Pacheco, J. E., Reilly, H. E. and Gregory, J., "Summary of the solar two test and evaluation program, Technical report, Sandia National Laboratories, SAND2000-0372C, 2000.
[4] Heller, L., "Literature review on heat transfer fluids and thermal energy storage systems in CSP plants," *STERG Report*, 2013.
[5] Yang, Z. and Garimella, S. V., "Molten-salt thermal energy storage in thermoclines under different environmental boundary conditions," *Applied Energy*, 87, No. 11, pp. 3322-3329, 2010.
[6] Garbrecht, O., Al-Sibai, F., Kneer, R. and Wieghardt, K., "Numerical Investigation of a new molten salt central receiver design," *SolarPACES 2012*, Marrakech, Morocco, 2012.
[7] Pacheco, J. E. and Dunkin, S. R., "Assessment of Molten-Salt Solar Central- Receiver Freeze-Up and Recovery Events," Technical report SAND96-0331C, Sandia National Laboratories, Albuquerque, USA, 1996.
[8] Kolb, G.J., "An evaluation of possible next-generation high-temperature molten-salt power towers," Sandia National Laboratories, *SAND2011-9320*, Albuquerque, NM, USA 2011.
[9] Kelly, B., "Advanced Thermal Storage for Central Receivers with Supercritical Coolants," Technical report DE-FG36-08GO18149, Abengoa Solar, Lakewood, Colorado, 2010.
[10] Raade, J. W. and Padowitz, D., "Development of Molten Salt Heat Transfer Fluid with Low Melting Point and High Thermal Stability," *J. of Solar Energy Eng*. 133, No. 3, pp. 31013-31016, 2011.
[10] Das, A. K., Clark, M. M., Teigen, B. C., Fiveland, W. A., and Anderson, M. H., "Heat transfer behavior of molten nitrate salt," *SOLARPACES 2015*, 1734, No. 1, 2016.
[11] J.W. Cooke and B. Cox, "Forced-Convection Heat-Transfer Measurements with a Molten Fluoride Salt Mixture Flowing in a Smooth Tube," Oak Ridge National Lab, 1973.
[12] Silverman, M.D., Huntley, W.R. and Robertson, H.E., "Heat transfer measurements in forced convection loop with two molten-fluoride salts: LiF-BeF2-ThF4-UF4 and eutectic NaBF4-NaF," Oak Ridge National Lab, 1976.
[13] Hoffman, H.W., "Turbulent forced convection heat transfer in circular tubes containing molten sodium hydroxide," Oak Ridge National Lab, 1952.
[14] Grele, M.D., Gedeon, L., "Forced-convection heat-transfer characteristics of molten sodium hydroxide," NACA, 1953.
[215] Hoffman, H.W., Cohen, S.I., "Fused Salt Heat Transfer - Part III: Forced-Convection Heat Transfer in Circular Tubes Containing the Salt Mixture NaNO2-NaNO3-KNO3," Oak Ridge National Lab, 1960.
[216] W. Yu-ting, L. Bin, M. Chong-fang, G. Hang, "Convective heat transfer in the laminar-turbulent transition region with molten salt in a circular tube," *Exp. Therm. Fluid Sci*., 33, pp. 1128–1132, 2009.
[217] Gnielinski, V., "New equations for heat and mass-transfer in turbulent pipe and channel flow," *Int. chem. Eng.*, 16, No. 2, pp. 359-368, 1976.
[18] Cabeza, L.F., "Lithium in thermal energy storage: A state-of-the-art review," *Renewable and Sustainable Energy Reviews*, 42, pp. 1106-1112, 2015.
[19] Fernández, Á. G., Gomez, J. C., Galleguillos, H., & Fuentealba, E., "Thermophysical properties and corrosion characterization of low cost lithium containing nitrate salts produced in northern Chile for thermal energy storage," *SOLARPACES 2015,* 1734, No. 1, AIP Publishing, 2016.

[20] Mohanty, B. P. and Shores, D.A., "Role of Chlorides in Hot Corrosion of a Cast Fe–Cr–Ni Alloy. Part I: Experimental Studies," *Corros. Sci.*, 46, No.12, pp. 2893–2907, 2004.
[21] Meier, G. H., and Pettit, F. S., 1989, "High-Temperature Corrosion of Alumina-Forming Coatings for Superalloys," *Surf. Coat. Technol.*, 39/40, pp. 1–17.
[22] Ma, J., Jiang, S. M., Gong, J. and Sun, C., "Behavior and Mechanisms of Alkali-Sulfate-Induced Hot Corrosion on Composite Coatings at 900°C," *Corros. Sci.*, 58, pp. 251–259, 2012.
[23] Glatzmaier, G. C. and Gomez, J.C., "Determining the Cost Benefit of High-Temperature Coatings for Concentrating Solar Power Thermal Storage Using Probabilistic Cost Analysis," *J. of Solar Energy Eng*., 137, No. 4, 2015.
[24] Kruizenga, A. M., "Corrosion mechanisms in chloride and carbonate salts," Sandia National Laboratories, Livermore, *CA Report No. SAND2012-7594*, 2012.
[25] de Miguel, M. T., Encinas-Sánchez, V., Lasanta, M. I., García-Martín, G. and Pérez, F. J., "Corrosion resistance of HR3C to a carbonate molten salt for energy storage applications in CSP plants," *Solar Energy Materials and Solar Cells*, 157, pp. 966-972, 2016.
[26] Ren, N., Wu, Y., Wang, T. and Ma, C. "Experimental study on optimized composition of mixed carbonate for phase change thermal storage in solar thermal power plant," *J. Therm. Anal. Calorim.*, 104, pp. 1201–1208, 2011.
[27] Olivares, R. Chen, C. and Wright, S., "The thermal stability of molten lithium-sodium-potassium carbonate and the influence of additives on the melting point, *J. Sol. Energy Eng*., 134, 2012.
[28] Mehos, M., Turchi, C., Vidal, J., Wagner, M., Ma, Z., Ho, C., and Kruizenga, A., "Concentrating Solar Power Gen3 Demonstration Roadmap", (No. NREL/TP-5500-67464). NREL (National Renewable Energy Laboratory (NREL), Golden, CO (United States)), 2017.
[29] Y. Wu, N. Ren, T. Wang and C. Ma, "Experimental Study on Optimized Composition of Mixed Carbonate Salt for Sensible Heat Storage in Solar Thermal Power Plant," Solar Energy, 85, pp. 1957-1966, 2011.
[30] N. Ren, Y. Wu and C. Ma, "Preparation and Experimental Study of Mixed Carbonates with High Maximum Using Temperature," in ES2012-91401, Proceedings of the ASME 2012 6th International Conference on Energy Sustainability, San Diego, CA, USA, 2012.
[31] CRU Group, "Lithium, The Problem With Prices", June 2016. [Online]. Available: http://www.crugroup.com/about-cru/cruinsight/Lithium-The_Problem_With_Prices.
[32] SQM, SQM's Thermo-Solar Salts (Salt Factsheet), Antwerpen, Belgium: SQM Europe, N.V. (www.sqm.com), 2016.
[33] Forsberg, C. W., Peterson, P. F., & Zhao, H. (2007). High-temperature liquid-fluoride-salt closed-Brayton-cycle solar power towers. Journal of Solar Energy Engineering, 129(2), 141-146.
[34] Haubenreich, P. N., & Engel, J. R. (1970). Experience with the molten-salt reactor experiment. Nuclear Technology, 8(2), 118-136.
[35] Williams, D. F. (2006). Assessment of candidate molten salt coolants for the NGNP/NHI Heat-Transfer Loop (No. ORNL/TM--2006/69). Oak Ridge National Laboratory (ORNL), Oak Ridge, TN (United States).
[36] Kruizenga, A.M., Kolb, W.J., Briggs, R.J., Christian, J.M., Ray, D.A., Gill, D., Kelton, J.W. and Chisman, K.M., 2014. Loop for the observation of film temperature effects on decomposition

(LOFTED) (No. SAND2014-18103). Sandia National Laboratories (SNL-CA), Livermore, CA, USA.

[37] Gill, D.D., Kolb, W.J. and Briggs, R.J., 2013. An evaluation of pressure and flow measurement in the molten salt test loop (MSTL) system. SAND2013-5366, US: Sandia National Laboratories.

[38] Pettit, K., Kolb, W.J., Gill, D.D. and Briggs, R.D., 2012. Customer interface document for the Molten Salt Test Loop (MSTL) system (No. SAND2012-1905). Sandia National Laboratories.

[39] Hobby, S., "Research continues on Solar with Molten Salt Storage," Renewable Energy World, 2014,http://www.renewableenergyworld.com/articles/2014/06/research-continues-on-solar-with-molten-salt-storage.html.

[40] Kruizenga, A. and Gill, D., 2014. Corrosion of iron stainless steels in molten nitrate salt. Energy Procedia, 49, pp.878-887.

[41] Doležel, I., Kotlan, V. and Ulrych, B., 2011. Magnetohydrodynamic pumps for molten salts in cooling loops of high-temperature nuclear reactors. Przeglad Elektrotechniczny (Electrical Review), ISSN, pp.0033-2097.

[42] Gill, D.D., Siegel, N.P., Bradshaw, R.W. and Ho, C.K., 2011, January. Design, fabrication and testing of an apparatus for material compatibility testing in nitrate salts at temperatures up to 700 C. In ASME 2011 5th International Conference on Energy Sustainability (pp. 605-610). American Society of Mechanical Engineers.

[43] McConohy, G. and Kruizenga, A., 2014. Molten nitrate salts at 600 and 680° C: Thermophysical property changes and corrosion of high-temperature nickel alloys. Solar Energy, 103, pp.242-252.

[44] Kruizenga, A.M., 2012. Corrosion mechanisms in chloride and carbonate salts. SNL Report.

[46] Pacheco, J.E., Showalter, S.K. and Kolb, W.J., 2002. Development of a molten-salt thermocline thermal storage system for parabolic trough plants. Transactions-American Society of Mechanical Engineers Journal of Solar Energy Engineering, 124(2), pp.153-159.

[47] Gill, D.D. and Kolb, W.J., "High Temperature Storage Loop: Final Design Report,", SAND2013-5365, Sandia National Laboratories, 2013.

[48] Wright, S.A., Conboy, T.M. and Rochau, G.E., 2011. Supercritical CO2 Power Cycle Development Summary at Sandia National Laboratories (No. SAND2011-6640C). Sandia National Laboratories (SNL-NM), Albuquerque, NM (United States).

Appendix A. Loop for the Observation of Film Temperature Effects on Decomposition (LOFTED)

2.2.1 LOFTED Overview

In 2014, the NSTTF designed and fabricated a pumped-salt test loop that was meant to initially flow molten nitrate salt through a heated test section of pipe and past a variety of material samples. The test system was developed to simulate operation over a 30-year plant life (estimated based on total salt volume and salt flow rate), with salt samples removed throughout the duration of the test. The salt samples, metal samples, and heated "receiver" tube were evaluated to study both salt decomposition over time and the effects of salt on system alloys. The receiver outlet temperature in its second phase was designed to operate at 600°C. The Reynolds number in the last panels of the receiver was designed to be nominally at 250,000. To achieve a bulk salt temperature of 600°C with a Reynolds number of 250,000, the salt film temperature was determined to be approximately 670 °C [36]. At or above this temperature however the salt would then thermally decompose, however, the residence time of the salt in the film region was believed to be too short for the decomposition reaction to proceed to completion. The capacity of the thermal storage system was designed to be approximately 14 hours where over the equivalent 30-year life, the salt inventory was designed to pass through the receiver approximately 16,200 times, exposing the inventory to the flux, and to the temperature conditions in the last panel, for a cumulative period of approximately 33 hours.

The salt used in the experiments was a nominal mixture of 60% by weight sodium nitrate, and 40% by weight potassium nitrate. The sodium nitrate was a typical industrial grade "Solar Salt", with a maximum total chloride content of 0.6%, and a maximum magnesium content of 0.1 percent. The potassium nitrate was a typical grade, with a maximum total chloride content of 0.2 percent, and a maximum magnesium content of 0.02 percent. Since the decomposition of salt was temperature dependent, the decomposition process accelerated when the salt moved from the bulk region to the film region, where the temperature of the salt could increase to the 670 °C limit. The decomposition process then would slow when the salt moved from the film region back to the bulk region, where the temperature of the salt decreased to 600 °C [36]. An experiment was developed to simulate the rate of decomposition that would be experienced in a potential commercial project.

2.2.2 System Design

The initial system design requirements were stated to:

1. Have a flow rate that met a Reynolds number similar to that for a CSP tower plant
2. Have the wall temperature maintained at 670 °C at the internal receiver wall
3. The coupons exposed to the outlet bulk-salt temperature of the heated receiver
4. Ensure that the salt inventory of the entire system would be as minimal as possible, such that the entire salt inventory could flow past the heated test section a predetermined number of cycles, so as to represent a 30-year power plant lifespan.

The experimental arrangement for LOFTED included a circulation pump, a heated test section, various instruments, and a control system. A representative piping and instrument diagram is shown in Fig. 2.2 where the pump drew suction from a pump sump, that circulated the salt through the pipe to the heated test section, and then returned it to the pump sump. A chiller fan system circulated air around the pump sump to reduce the temperature of the heated salt to the nominal bulk salt temperature. The pump sump was maintained at a nominal temperature of 600°C by balancing the heat input from the test section with the heat removed by the fan. The experiment was designed to use a heated tube (representative of the actual solar heat flux receiver) with an inside diameter equal to that of the commercial receiver (41 mm), and to operate with a nominal salt flow velocity of 3 m/sec. An unheated section of pipe, with a diameter of 41 mm and a length of 11 m, was installed upstream of the test section where its purpose was to establish a hydraulic boundary layer, similar to that at the mid-point of a commercial receiver panel. Here, the commercial receiver and test section had in theory comparable values for the Reynolds number, the velocity profile across the tube diameter, the fluid temperature profile across the tube diameter, and the oxide production rate per kg of flow. The method used to heat the test section of receiver is to pass a high-frequency, oscillating current through an electric coil surrounding the tube. This establishes a film temperature of 670°C, for which a nominal input power of 75 kW_e per meter of heated length is required.

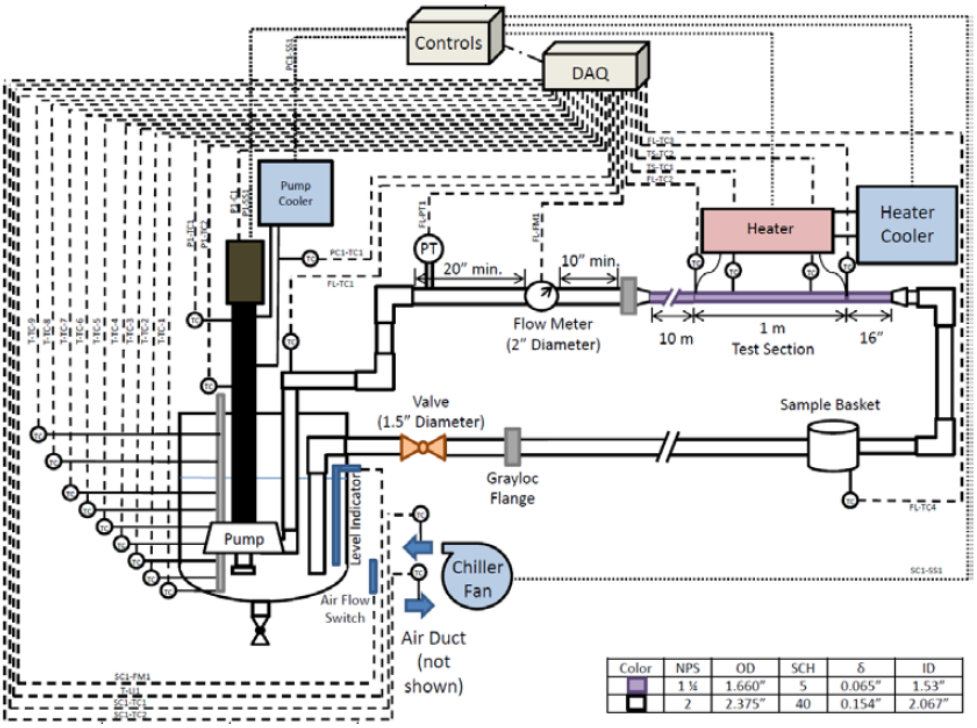

Figure 2.2. LOFTED piping and instrumentation diagram [36].

The pump and test section at the end of the system is shown in Fig. 2.3 which provides a visual of the platform that was modified to support the tank, pump, pump motor, and pump bearing cooler. A set of stairs was constructed for safe access to the platform during salt sampling. The pump was placed on an interface plate, which was attached to a small molten salt tank built from

a .66 m (26”) diameter 316 SS pipe. The salt within the tank was electrically heated by externally mounted mineral-insulated (MI) heat traces. There were thermocouples (TCs) mounted internally to the tank, which allowed for salt level monitoring, as well as molten salt temperatures and upper air temperatures within the tank. The level was also measured using a bubbler system [36]. The pump feeds the supply piping, where the salt flows past a pressure transducer and through a flow meter to the supply side is 2 in. NPS schedule 40, 316 SS pipe. After turning through two long-radius elbows at the end of the pipe, the salt returns to the tank through Haynes 230, 1.5” tubing. Attached to the second elbow is a reducer measuring 2 inches to 0.5-inches. The Haynes 230 1.5-inch, schedule 5 tubing was attached to the reducer. This tubing represents a section of an actual commercial receiver. There were three sections within the Haynes 230 receiver: the pretest section, measuring 10.97 m in length, the 1 m test section, and a 0.41 m post-test section. The Haynes 230 was welded using Haynes filler rod. The tubing had a 10.97 m free flowing zone, simulating a half-length of receiver piping, before entering the 1 m induction heated zone (inside the protective shed), where heat was added through the surface of the pipe to achieve a higher film temperature. This coil, along with the associated electrical and controls, provided the required thermal input to the receiver tube to obtain the 670°C internal wall temperature. The post-test tubing continues to maintain a steady flow before passing through a control valve, the metal sample test section, and before being sent back into the tank. The pump, pump motor, control valve, and blower already existed on-site, and were repurposed for this test.

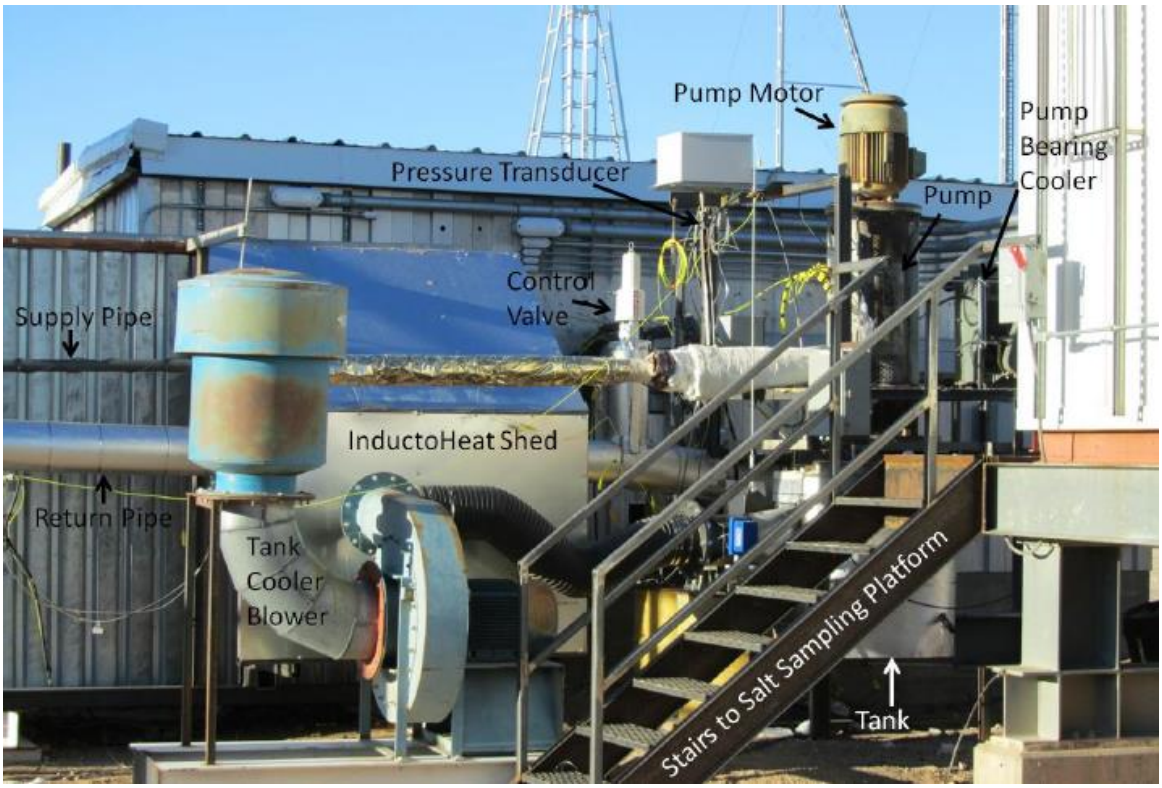

Figure 2.3. The LOFTED Pump and Test Section Installed at the NSTTF [36].

Accordingly, Fig. 2.4 shows a broader view of the test system that includes the flow meter and turn-around sections of the piping, as well as the pipe hangers. Because the pipe length increases by 8.9 cm during heating to a predefined operating temperature, the pipe hangers were all made to be compliant to longitudinal motion. The supply pipe was much stronger than the return tubing, so the supply pipe used more traditional pipe hangers welded to the pipe. The return tubing was supported in hanging pipe cradles, first, because the tubing was quite flexible, and second, because of the desire to have a smooth, free-flowing tubing for developing the flow regime. All piping runs contained a slope of the pipe, providing positive flow for the salt to drain back to the tank when the system is shut down.

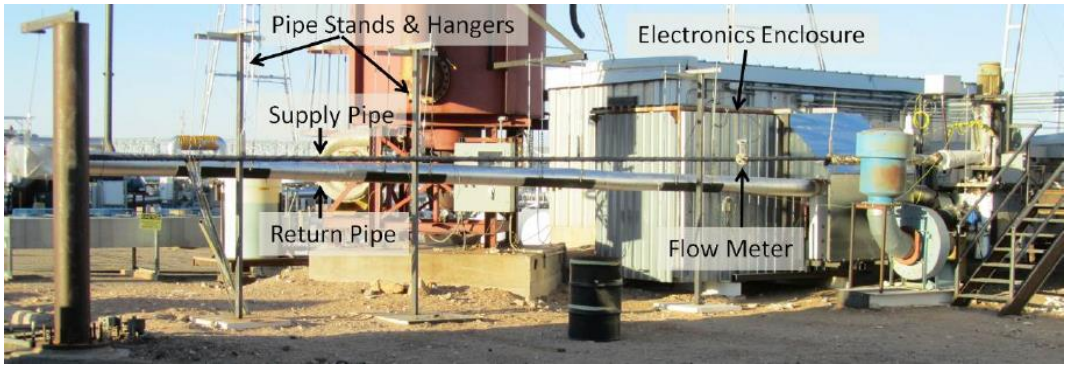

Figure 2.4. View of the LOFTED system, showing the full piping system and pipe hangers [36].

From Fig. 2.4 it is evident that the supply line was not insulated, while the return line was. The system was originally constructed with both lines insulated and heat-traced where it was brought to temperature with subsequent flow being started [36]. However, it then became necessary to de-insulate the supply line to achieve additional cooling to reject the heat generated by the induction heating system, which was meant to get salt up to film temperatures as high as approximately 650 °C-750 °C. Fig. 2.5 shows the back side of the electronics enclosure, which contains the controller and pyrometer for the InductoHeat unit. The enclosure protects these items from rain. The InductoHeat requires substantial cooling for the coil and the control electronics, therefore the enclose is equipped with a primary cooling loop that cools these items, as well as with a heat exchanger on a secondary loop [36]. The secondary loop consists of a pump cart with a large volume of coolant and an air-to-water fin-fan heat exchanger. All of these items, including the electronics enclosure, existed onsite at Sandia, and were repurposed and adapted for use during this test.

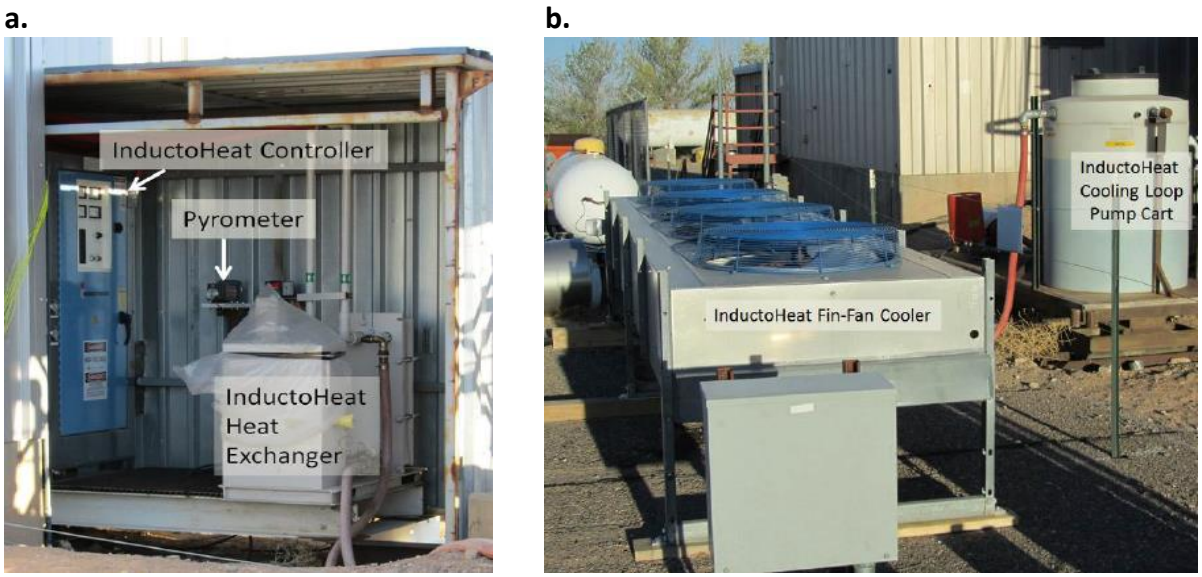

Figure 2.5. a. Electronics enclosure with InductoHeat controller, pyrometer, and heat exchanger, and b. connected cooling loop and cooler [36].

The tanks and piping were all lined with mineral-insulated resistive heat trace. Stainless steel shimstock was used to secure the heat trace in place, and a layer of shimstock was wrapped around each vessel to isolate the heat trace from the insulation. The primary insulation is Pyrogel XT, in 5 and 10mm thicknesses, with some Thermal Ceramics Superwool used to fill small gaps. A layer of shimstock was installed partway through the insulation layers to reflect IR emissions back into the piping system. Finally, the vessels were covered with a layer of aluminum cladding for weather protection.

2.2.3 SubSystems

2.2.3.1 The Tank

The tank, Fig. 2.6 with a NPS 26-inch diameter, was constructed of 316 SS. The tank temperature tree provided the internal salt and air temperatures at 4-inch intervals from the bottom to the top of the tank, with additional TCs spaced ½-inch apart between 15-18 in. from the tank bottom. This lower region had more T/Cs to provide additional sensing at the operational salt level during normal operations, nominally 17 inches. A pipe flange was welded to the upper portion of the 26-in. pipe, which was bolted to a stainless-steel interface plate.

Figure 2.6. The tank positioned in the assembly stand, with flow control valve and cooling ductwork.

2.2.3.2 Molten Salt Pump System

A Lawrence 25 HP cantilever molten salt pump flow rate of 100 gpm, with 100 PSI at 600°C was employed as the pump for this system. The pump did not control flow or pressure in the system where it had a pipe flange welded to its base. This flange was bolted to the stainless steel interface plate. The pump would automatically shut down if any of the set-point values outlined in the alarm matrix are reached. Additionally, the Lawrence pump required an auxiliary radiator and water pump, which facilitated water flow through the thrust bearings to keep them cool. This pump cooler system ran continuously where an automatic trip of the salt pump would occur if the water temperature rose higher than the set-point value. Finally, the pump and tank interface plate, was made of 347 stainless steel, which was required to isolate the carbon steel pump flange-plate from the high temperature salt, Fig. 2.7.

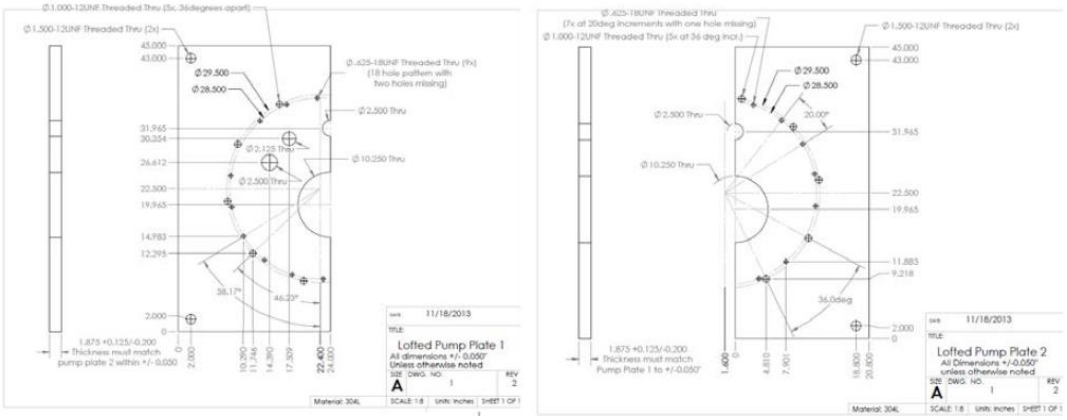

Figure 2.7. The 347 SS plate that supported the pump and the tank, where the plate is configured as two halves that slide together around the assembled pump [36].

2.2.3.3 Test Section & Piping

The test section was constructed as a 1 m NPS 1-1/2 in. Haynes 230 (1.6 in. OD), as shown in Fig. 2.8, the test section was encapsulated by the InductoHeat coil. The rest of the piping system consisted of several types of materials: all NPS two-inch pipe was 316 SS schedule 40, the flow meter was 321 SS, the PT extension was 316 SS, where the pretest, test, and posttest sections were Haynes 230, 1.5 in., schedule 5 tube. A 4 in. 316 SS pipe held metal test section coupon samples.

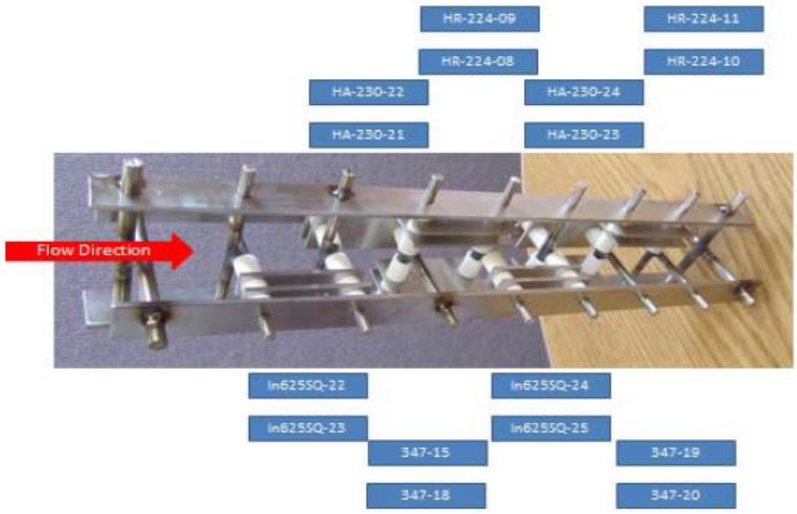

Figure 2.8. Test section sample tree containing metal samples in flow stream for corrosion analysis [36].

2.2.3.4 Induction Heater and Heat Trace

The test section was heated via a 150 KW InductoHeat induction heating unit, Fig. 2.9. The unit heated the surface of the test section to a set point of 670 °C, which was controlled via LabVIEW

PID controls [36]. The induction heater was controlled using a 0-10 VDC signal input. The InductoHeat unit was selected as it can apply a large amount of thermal energy to a very small area of material. The InductoHeat unit and coil were comparatively expensive, with low efficiency, but was available on a commercial basis, where it provided a uniform heat flux around the circumference of and along the length of the tube. Comparatively, resistive heat trace could not achieve the power density needed in the small area where radiant heaters presented problems with flux uniformity and lamp cooling.

a.

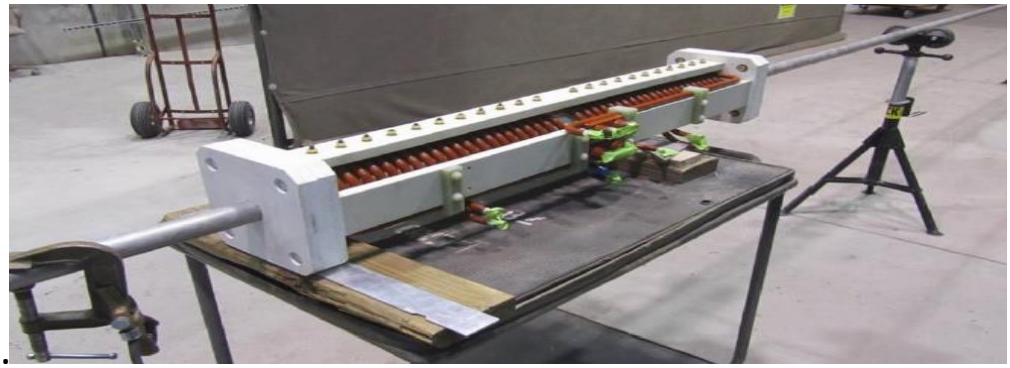

b.

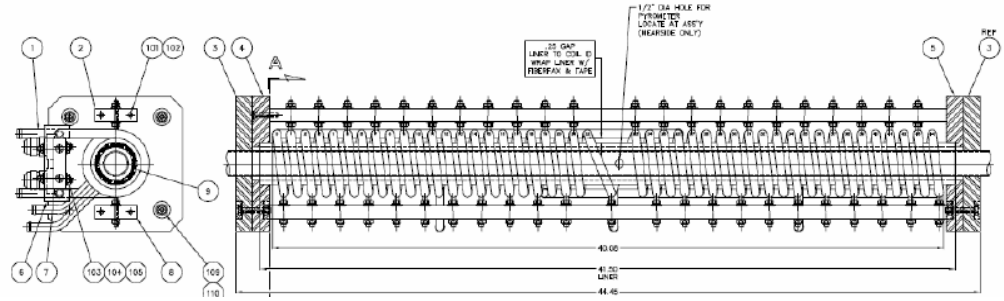

Figure 2.9. 1 m InductoHeat coil supported by insulation board, where Haynes 230 tube is surrounded by rigid insulation.

To maintain operational temperatures, the piping system was heated using five separate electrical heat trace cables, which were used to heat the 1. pump discharge to the pre-test section, 2. pressure transducer (PT) extension [36], 3. pre-test section, 4. the valve bonnet, and 5. the test section to the tank inlet, which includes the coupon sample holder and the valve body.

2.2.3.5 Instrumentation and controls

The instrumentation and controls sub-system supported both automatic/manual control and monitoring of the Lofted system. Data was collected at 30 sec intervals, and was saved to a unique spreadsheet at 12 midnight. The system was composed of the following components:

- Desk-top computer and monitor
- Network connected National Instruments (NI) Compact RIO (cRIO-9072)
- NI C-series modules to support digital and analog IO to/from the Lofted hardware.
- Signal isolation modules (where appropriate) to protect the NI modules from surge damage.

- Uninterruptable Power supply to maintain control and monitor of the system, over short (10-15 min) power out periods.

A GEFRAN 750 PSI NAK pressure transducer, Fig. 2.10 with a 6 in. flexible stem was used which provided a 4-20 ma analog input to the NI control system. The pressure transducer was mounted to a 316 SS extension standoff pipe, 30 inches long, with a ¾ in. diameter. This extension was intended to lower the temperature of the salt within the 2-in pipe (600 °C to 300 °C at the diaphragm of the pressure transducer). The pressure transducer electronics was located in a NEMA 4 box containing an electric heater controlled by a thermostat to maintain 55 °C, which was necessary to provide a constant temperature to the electronics that helped eliminate daily shifts in data due to temperature swings in the ambient environment. The pump and heater would automatically shut down if any of the values outlined in an alarm matrix were reached.

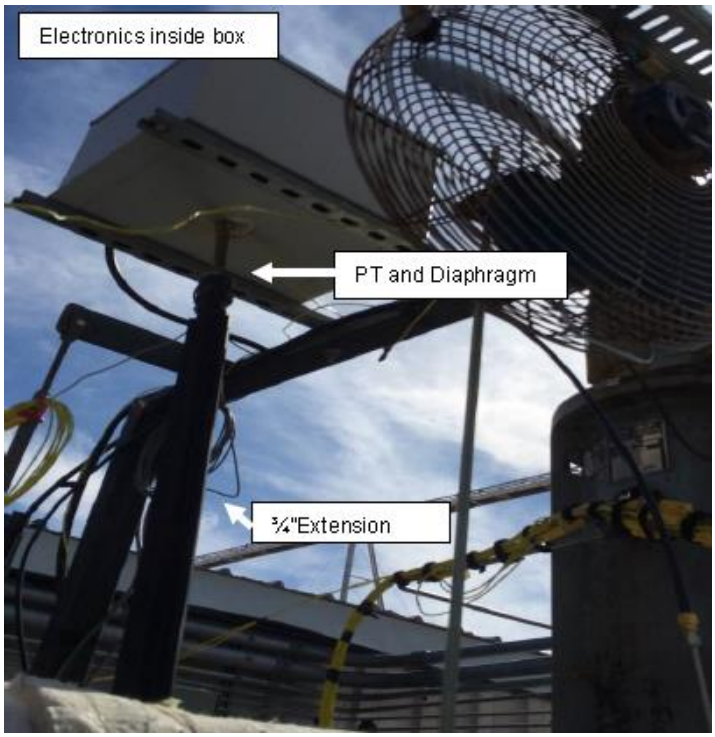

Figure 2.10. Pressure Transducer mounted on 30" extension [36].

A Krohne ultrasonic 2-inch molten salt flowmeter, (Model # S39447X303D00100, 321 H SS) was employed for the flow tube, Fig. 2.11, with the addition of a converter: VN5045D0032300010. The flowmeter provides a 4-20 ma analog input to the NI control system. The flowmeter was welded into the 2 in. piping system and the converter was mounted approximately 4 m away within the associated building. The pump and heater automatically shut down if any alarm matrix values are reached.

a.

b.

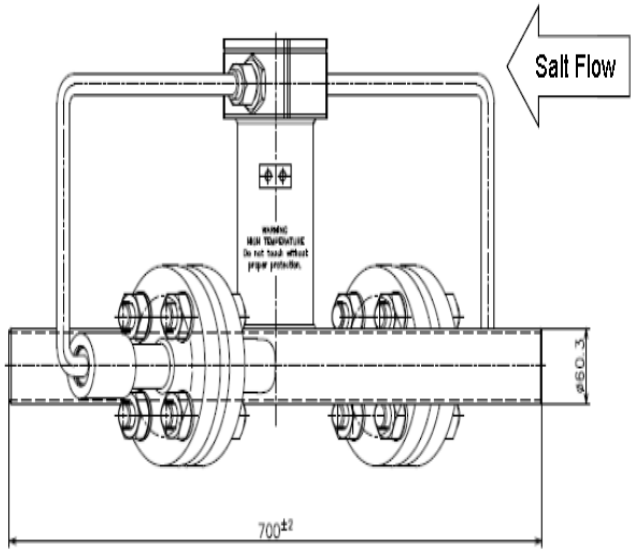

Figure 2.11. LOFTED a. Flowmeter electronics are mounted separately, away from the heat and b. flow meter directional schematic [36].

2.2.3.6 Operation, Test Results and Discussion

The first test was initiated on April 8, 2014 where much experience was gained in high-temperature operation with molten nitrate salts. Initially, each control and data signal was tested from end-to-end, and the functionality of the control and data acquisition systems was confirmed. The tank was heated and salt was introduced and melted using the tank heaters. A total of 775 lbs. of solar salt was added to the tank through the vent line located on top of the tank. A combination of 475 lbs. of sodium nitrate (NaNO3) prills (60%), and 300 lbs. of potassium nitrate (KNO) prills (40%), were added. The solar salt used for this test consisted of 60 % NaNO3 Industrial Grades Prills and 40% KNO Technical Grade Prills purchased from SQM North America Corporation. Once all of the salt had been introduced and was melted, the temperature was raised above 500 °C for 48 hours, then raised to 585°C to decompose any magnesium nitrate to magnesium oxide [36]. After this operation and testing began where valuable experience was gained in working with design of molten salt systems.

Flange and bolted connections in molten salt systems are known to be sources of salt leaks. This is mainly due to incompatible materials used for gasket materials and the elongation of bolts due to thermal cycling (i.e. expansion and contraction of the metals). Bolt growth can facilitate a leak path to form wherein salt may permeate. Initial salt technology surveys, prior to designing the LOFTED system, led to the selection and use of Grayloc hubs, 316 SS, Schedule 40, 2-piece, 4-bolt clamps and seal ring, Inconel 718, silver. Operational experience from this test indicates that current salt technology has not adequately addressed this leak issue and all connections should continue to be welded in the future. Similarly, a pump and tank interface plate was designed allowing separation of the carbon steel pump plate from the 600 °C molten salt. This plate was bolted to both the tank and to the carbon steel pump plate. This interface plate also allowed

placement of the pump into the tank. This plate was welded to both the carbon steel pump plate and to the tank to avoid leaking issues.

The GEFRAN pressure transducers have not operated well in our other system at the NSTTF due to excessive heat at the diaphragm and the electronic components. These issues resulted in leaks at the bolted connection, inaccurate readings. Past attempts to thermally isolate the transducer from the molten salt by placement of a long standoff tube resulted in a Venturi-effect, causing a vacuum, which caused the diaphragm to fail [36]. This problem was solved by placing connecting a ¼ inch tube from the diaphragm and extending approximately 1/8 inch into the molten salt flow. The ¼ inch was placed inside of a 30-inch-long ¾ inch diameter pipe that was allowed to leak slightly at the cold connection. Operational experience indicated that these design changes alleviated heat and vacuum issues, however more testing is needed to verify any resultant changes in accuracy. The Krohne flow meter operated continuously with a salt inventory at 600 °C. The reading from the meter appeared to be very consistent over the entire test period. The flow meter was not insulated, which allowed it be in thermal contact with surrounding and operate at temperatures lower than 600 °C.

2.2.3.7 Current Status

Initially, the intent of this project was to understand if you could push the limits for current solar salts and understand the instrumentation and controls challenges associated with high-temperature operation. Currently LOFTED is no longer operational, but a replicate system could be built considering the experience and current salt flow-equipment capabilities at the NSTTF, which could be setup for chlorides, fluorides and carbonates with added changes to the system design, which include cover gas piping, connections, controls and instrumentation. The costs to do this would be dependent on the heating source and the type of salt used for testing as the materials could vary significantly. Approximate cost estimates for refurbishment of this capability range between $500k-$1M.

Appendix B. Miscellaneous Molten Salt Capabilities

2.4.1 Corrosion Analysis Capabilities

Increasing the temperature limit within the molten salt hot tank requires a detailed understanding of materials corrosion behavior, in addition to salt thermal stability properties. The NSTTF extended research group, in connection with the Sandia-Livermore site in Livermore, CA, have conducted much work in the areas of molten salt corrosion and materials characterization degradation analysis. Static immersion tests conducted by Kruizenga et al. [40] have previously been performed at the NSTTF [42]. Here, flat coupon samples were immersed in binary nitrate salts at temperatures of 400, 500, 600, and 680 °C, with air sparging on all tests. Test samples were mounted on sample trees and separated by ceramic beads, then immersed in the binary solar salt at a given temperature. Air was sparged through a cross drilled tube to provide mixing of the salt and ensure that the partial pressure of O_2 was consistent throughout the course of the experiments, for the sake of salt chemistry through the nitrate/nitrite equilibrium. Samples were nominally removed at intervals of 500, 1000, 2000, 3000 and 4000 hours to acquire data on time varying weight gain information while simultaneously employing metallography to identify corrosion mechanisms occurring within the melt. The purpose of this test was also to provide initial data on relative performance between these alloys and to determine changes in corrosion mechanisms as a function of temperature.

For the test, test samples were mounted on sample trees and separated by ceramic beads, then immersed in the binary nitrate salt at a given temperature. Air was sparged through a cross drilled tube to provide mixing of the salt and ensure that the partial pressure of O_2 was consistent throughout the course of the experiments, for the sake of salt chemistry through the nitrate/nitrite equilibrium. As shown in Fig. 2.22 oxide formed tenaciously on high-nickel content alloys, which were not easily removed using mechanical or chemical techniques alone.

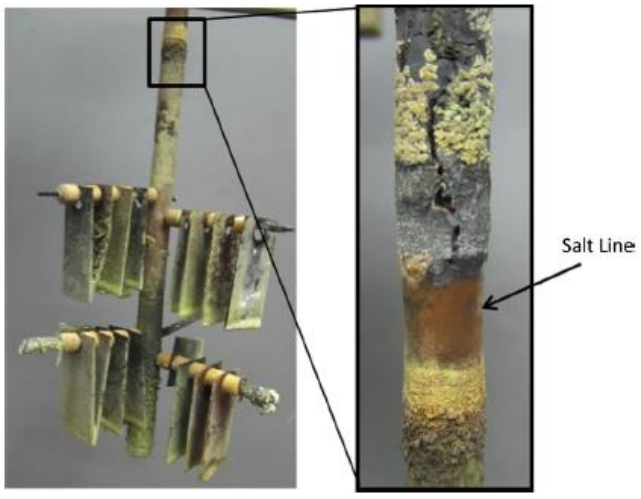

Figure 2.22. Sample tree and samples after exposure in 680 °C salt [43].

Thermal impurity analysis of salts has also been performed where impurities produce a difference

in the visual appearance of the salt as shown in Fig. 2.23. Accordingly, Table 2.3 summarizes the composition of the aged salts and measured thermophysical properties which show measurable differences in heat of fusion and melting point compared to the unaged molten nitrate salt.

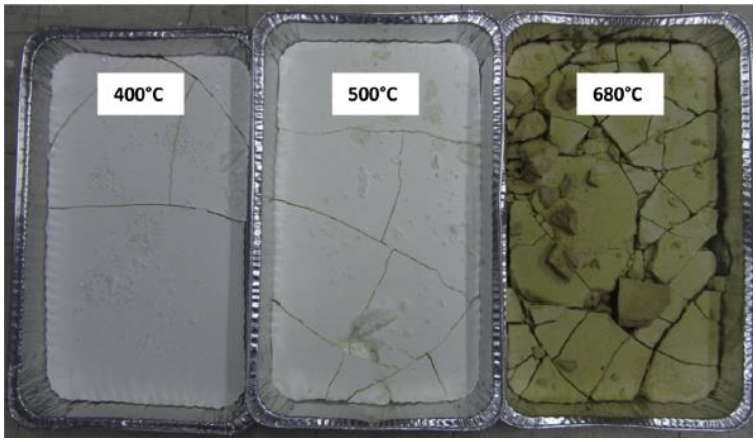

Figure 2.23. Appearance of molten salt after extended operation at different temperatures [43].

Table 2.3. Thermophysical properties for conditions of solar molten salt at 600 and 680 °C [43].

Operating temperature (°C)	Time at 680 °C (h)	Heat of fusion (J/g)	Specific heat at 327 °C (J/g K)	Melting point (°C) (from DSC)	Liquidus point (°C) (from Optimelt)	Liquidus point (°C) (from DSC)
Literature values (Rogers and Janz, 1982)	0	112 ± 1	1.59 ± 0.03	225 ± 1	245 ± 1 (DSC measurement)	245 ± 1 (DSC measurement)
NA	0	107 ± 1.5	1.77 ± 0.16	220 ± 0.29	242 ± 3	244 ± 4
680	520	85.3 ± 2.3	1.60 ± 0.22	161 ± 1.5	213 ± 3	209 ± 4
680	1025	74.6 ± 3.3	1.83 ± 0.59	151 ± 1.5	Indeterminate[a]	200 ± 4
680	2000	69.1 ± 2.2	1.63 ± 0.59	156 ± 0.7	202 ± 3	197 ± 4
600	1000	94.2 ± 6.2	1.53 ± 0.09	192 ± 0.6	231 ± 3	243 ± 4
600	3000	90.4 ± 0.65	1.95 ± 0.34	190 ± 0.5	227 ± 3	227 ± 4
600	4000	89.4 ± 2.2	1.55 ± 0.12	192 ± 0.3	228 ± 3	227 ± 4

[a] This value was unable to be determined because of large displacements of the molten salt during heating, which rendered changes in phase undetectable.

Microscopy capabilities at SNL can also be employed to determine relevant corrosion reactions that occur during molten salt exposures to various stainless steels and Ni-based alloys. Scanning electron microscopes (JEOL JSM 840A) equipped with energy dispersive spectroscopic systems (Thermo Electron Corp) have previously been used where generated images are used to correlate the presence of an element within a given area. The relative amount of an element present is related to image contrast; dark maps indicate little to none of the elemental species present, while bright maps correspond to high elemental concentration. Additionally, electron microprobe (EMP) can also be employed, Fig. 2.24 to gain quantitative concentration data as a function of location. X-ray diffraction (XRD) (PANalytical Empyrean) and goniometer modes can be used on alloys with thick oxides for the determination of surface corrosion phase.

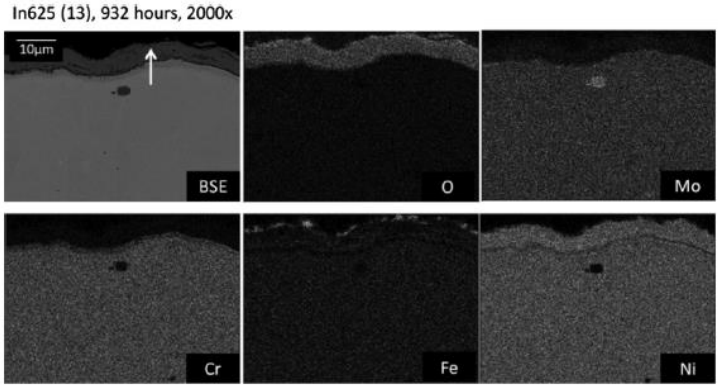

Figure 2.24. X-ray map and EMP data for In625 after 932 h of exposure at 600 °C to solar salts where the oxide structure is primarily composed of a 5–8 lm nickel oxide, with a thin layer of iron oxide on the outermost portion of the oxide [43]. However, previous research has found that alloys with thin or less-dense corrosion products, such as hematite or magnetite can sometimes prove more difficult to measure, though solutions do exist to make these measurements [43].

Research has also been previously performed by SNL-Livermore for analysis of other molten salts such as chlorides and carbonates, which can also be extended to fluoride salts [44]. Chloride and fluoride salts are susceptible to high corrosion rates in the presence of moisture and oxygen. Purification techniques have previously been examined and are extremely important to ensure good materials performance, as formation of protective layers does not readily occur [44]. Research for these types of purification techniques can be extended from chloride to fluoride salts in addition to compatibility research for cover gases used within fluoride molten salt reactors. Materials performance and reliability expertise and capabilities at SNL include static, tilted table, natural convection, and forced convection corrosion tests which have been performed using a variety of SS and Ni-based alloys and ceramics, which can be extended for fluoride salts [44].

2.4.2 Molten Salt Thermal Storage & Test Pots Capabilities

Thermal storage systems are an important part of solar thermal power plants. Thermal storage allows power to be dispatched, where tests of various systems are being conducted in an effort to improve the marketability of the technology [45]. As opposed to a two-tank molten-salt storage system, thermocline molten-salt systems store energy in a single tank containing a filler material. Inexpensive filler materials replace costlier nitrate salts where R&D efforts for these lower-cost systems have been conducted since 1999 at the NSTTF evaluating thermal cycling resilience of several different solid mediums exposed to molten salt and to address the mechanical integrity of filler materials subjected to thermal shock that could be experienced in a thermocline storage tank. Thermal cycling and accelerated-life tests were conducted with NSTTF thermocline test facility capabilities, Fig. 2.25 where samples were held in a vessel and molten salt was passed through the samples from two tanks. The tests showed that quartzite and silica sand best held up to the cycling with nitrate salt, which from the investigation were the most economical, and are more readily available than other materials tested 46].

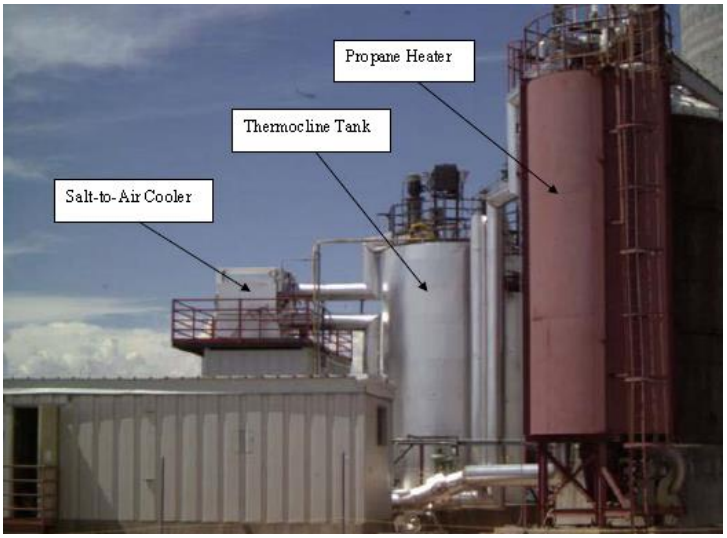

Figure 2.25. NSTTF thermocline test facility capability [45].

Some thermal cycling tests were able to provide accelerated life time information for the tested materials for an equivalent 30-year operation.

Fig. 2.26 depicts the basic arrangement for the thermal cycling apparatus for testing material compatibilities with system alloys at the NSTTF. The entire system was constructed using welded 316 stainless steel piping and components. A small 10.2 cm diameter test chamber 35.56 cm tall containing filler material was placed between two vessels—the hot and cold tanks—each 25.4 cm diameter by about 152 cm tall. The hot tank was designed to contain molten salt at 450°C and the cold tank at about 285°C [46]. Two gate valves and a drain valve were installed for periodic isolation and draining for sample observations. After mechanical fabrication, the entire system was carefully heat traced, thermocouples were installed, and the system was insulated to minimize heat loss while still allowing thermal cycling to occur. The filler medium test chamber and components were carefully fabricated to ensure containment of the mineral/sand samples while still allowing molten salt flow in either direction during thermal cycling [46].

a.

b.

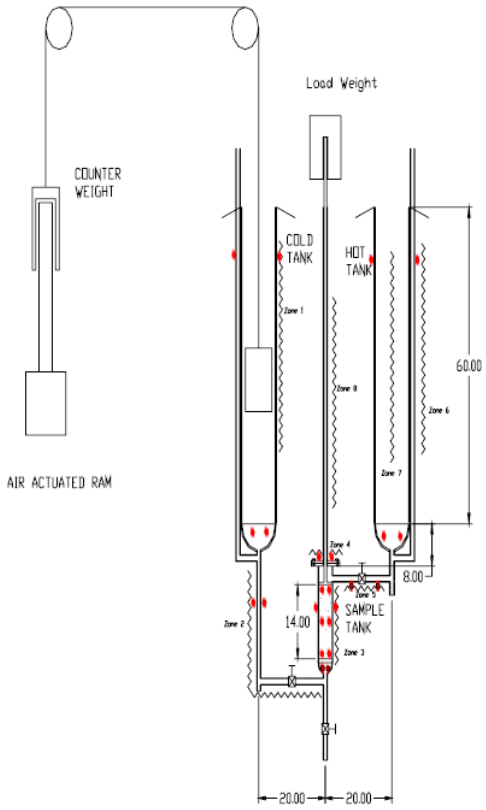

Figure 2.26. a. Thermal cycle insulated test apparatus and b. Test chamber and valving for filler materials tests [45].

The salt pot tanks are material testing tanks that are capable of heating salts to 600 °C or more depending on the set conditions. The tanks are currently made from 321 Stainless Steel with internal heating rods to heat the salts. The tanks are well insulated and can be used for continuous operations. Material samples are placed on "trees" that are inserted into the molten salt. The material samples can be removed periodically to determine corrosion or other heating effects. There are three tanks that can be used for these experiments. SNL have used these pots for internal DOE studies for molten salts. SQM has also used this experimental setup to evaluate the effects of heating on different salt types and materials that can be used with those salts.

This experimental setup is a low-cost experiment with most of the cost being startup. The "trees" are often custom fit for the type of material sampling required. A typical test including startup could range from $20k-$100k depending on the test setup and duration of testing with required intervals to check on the material samples. Previous research with these salt pots have included isothermal tests to evaluate the long-term durability of quartzite rock and silica sand statically immersed in ternary molten salt at both 450 and 500 °C. Four melting pots, Fig. 2.27 are included–two at the test temperatures with samples, and two control pots at test temperatures without samples. Here, the melting pot Chromalox controllers were visually monitored on a daily basis to ensure setpoint temperatures were maintained. Three 316 SS sample baskets are made up for each of two salt pots (consisting of a 2:1 mixture by weight) of quartzite rock and silica sand, quartzite rock alone, and silica sand alone, respectively.

Figure 2.27. Isothermal Molten Salt Test Posts at NSTTF [45].

Zones 1 and 2 within Fig. 2.27 contained the rock and sand samples in molten salt which were carefully washed, dried, weighed, and photographed prior to insertion in the melting pots. The ‘‘control’’ pots without samples—Zones 4 and 5—are established at the same temperatures. Because of supply limitations, half the quantity of salt is typically melted in the control pots. This results in an identical molten mixture, but also a doubling of the effective surface-volume ratio in these pots as compared to the Zones 1 and 2 pots containing the samples. Over time, rock and sand samples are removed, observed and weighed, and salt samples are taken for chemical analysis. Shutdown of the isothermal tests is quite simple. Final salt samples are taken, and the final process of extracting, rinsing, drying, weighing, and photographing rock and sand samples occurred. The rock/sand samples were then bagged and labeled for eventual detailed analysis by Sandia experts. Fig. 2.28 shows the typical nature of the crust that formed on the surface of the molten salt in the Zone 5 control pot, here with nitrate salt at 500 °C [45].


Figure 2.28. Isothermal test with typical crust formation, within the Zone 5 test pot [45].

An important condition to note: other than convective currents in the pots, none of the pots are mechanically stirred or plumbed for flow conditions for the duration of testing, so these are truly static tests [Brosseau, 2005]. These tests provide valuable information regarding the ability of potential compatible construction or filler materials to withstand test conditions in a molten salt, and they also provided direct observations of changes in molten salt. This capability could be directly used between fluoride salts and molten salt reactor components and materials.

2.5 High Temperature Storage Loop

2.5.1 Overview

A research scoping plan was developed at the NSTTF which included a strategic goal of providing a test capability for SNL to evaluate high temperature storage (>650°C) technology [47]. This effort was to scope, design, and build a flow loop that would be compatible with a multitude of high temperature heat transfer/storage fluids including high-temperature molten salts, which may include chloride, fluoride or carbonate molten salts. The High Temperature Storage Loop (HTSL) could be reconfigurable so that it is useful for not only storage testing, but also for high temperature receiver testing and high efficiency power-cycle testing. Therefore, HTSL was part of a much larger strategy for the NSTTF to provide a research and testing platform that would be integral for CSP, or other high-temperature applications in the evaluation of individual technologies or systems. The primary objectives for the effort were to provide a flow test capability for the evaluation of high temperature thermal energy storage (TES) heat transfer fluids (HTF). Additionally, this system would provide a storage test bed for analyzing storage methodology at high temperature within an operating temperature range of 250-800 °C [47]. This capability would also provide a flowing test bed for performance analysis of storage components including piping, valves, flanges, instrumentation, and the associated equipment necessary for these components (e.g. packing, gaskets, and seals) for flow rates less than that of MSTL. This capability would also provide a HTF/heat removal capability for tower-top receiver testing where the system could be tested on top of the Sandia NSTTF solar tower facility, with cooling needs up to 1.0 MW_{th} [47]. This system was designed to be modular on a skid so it should be relatively self-contained so it can easily be loaded onto the NSTTF tower module and attached to receiver and or cooler skids for use at the top of the tower. The skidded nature would allow the most expedient and cost-effective testing to be done by allowing the skid to be placed in the most opportune location for a test.

2.5.2 Design Constraints

The design targets as shown in Table 2.4 provides the Design Criteria with the target values for the design system. For the system flow rate, a common rule of thumb taken during the design process for preventing pipe erosion was to keep the flow speed of the fluid less than 10 ft/s. For 1.5” pipe, the maximum volumetric flow rate would therefore be 55 gpm and for 2” dia. pipe, the maximum volumetric flow rate would be 97 gpm. The pipe diameter will be further reviewed during the detailed design process to accommodate system effects such as preferential material

transport, especially found in chloride applications, and also corrosion effects and barrier coating requirements.

Table 2.4. The design criteria with target values and a range of acceptable values [47].

Design Criteria	Target Value(s)	Acceptable Value(s)
Temperature Range for Testing	250°C – 750°C	450°C-700°C
Thermal Input/output	700kW$_{th}$	500kW$_{th}$ – 1MW$_{th}$
System Flowrate	6.2 kg/s (~50gpm)	4.9-8.6kg/s (~40-70gpm)
Temperature Delta	200°C	100-300°C
Pump Pressure	53m H_2O (75psi) minimum	53-88m H_2O (75-125psi)
Piping	1.5",high nickel alloy	1.5-2" (2" nec. If flow>55gpm)
Storage Vessel(s)	3.8 m^3 (1000gal) Can be Pressurized to 1ATM	2.7-7.6 m^3 (700-2000gal.)
Storage Vessel(s)	1 tank w/ high temp capability	1 hot & 1 cold tank
Gravity Drainback	Slope ¼" per foot	Slope 1/8" per foot
Skid Mounted	1 skid for TES loop	Cooler or Receiver on separate skids

The amount of heat that can be absorbed in the fluid depends on the fluid's specific heat, the desired temperature change, and the flow rate of the fluid. The decision of the design temperature difference between hot and cold sections is relative for a fluid for a given test loop/power cycle. For example, the supercritical CO_2 power cycle promises high efficiency with small turbine equipment. The Sandia 700kW split flow [48], simple cycle with recuperation takes heat from a heat source over a 150 °C range from 450-600°C with the remainder of the cycle's heat being supplied by recuperation. Additionally, system pressure would need to overcome piping loss through the system as well as meet the head requirements of any receiver tests. Friction/restriction loss through a heater, cooler, valves, and piping is expected to be less than 50 psi for this design [47].

2.5.3 System Configurations

Fig. 2.29 provide potential system configurations that could be realized for this system. Although the solar receiver and power cycle are shown, they would not be part of the initial construction, where heat input may come from induction heating. However, these figures show the ability of the system to be used in the testing and validation of other subsystems. In each system design, the heater and receiver could be interchanged, where too the cooler and power cycle could be interchanged.

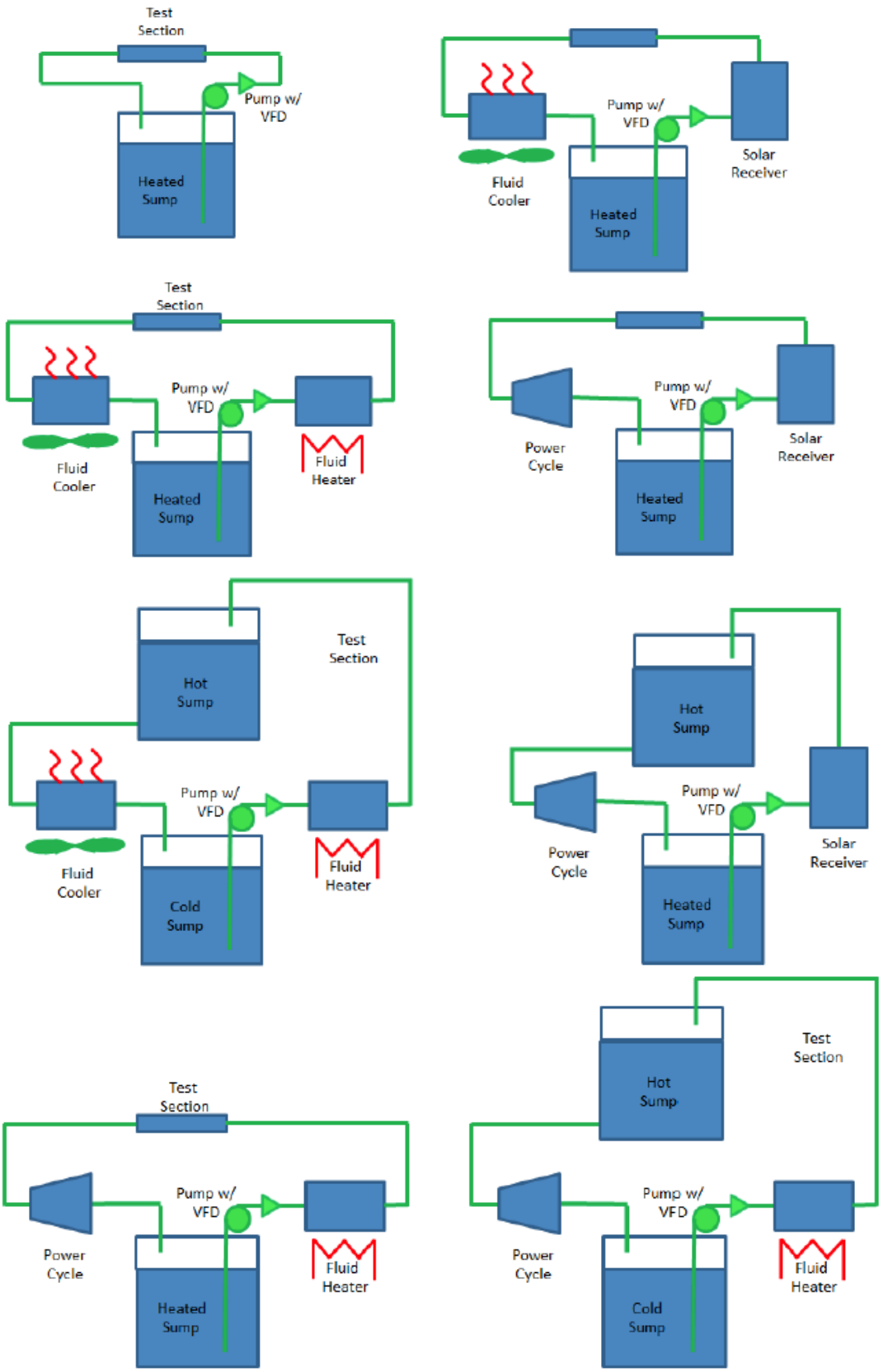

Figure 2.29. HTSL Potential Test Configurations of the High Temperature Storage Test Loop [47].

2.5.4 System Design

2.5.4.1 Overview

This design required modularity so that the system is adaptable to many of the configurations identified in the scoping activities. The design was modified as necessary with respect to component and fabrication costs, which addressed [47] the actual scale of different components was determined. An isometric view of the design is shown in Fig. 2.30. Note that all of the piping is shown without insulation for clarity.

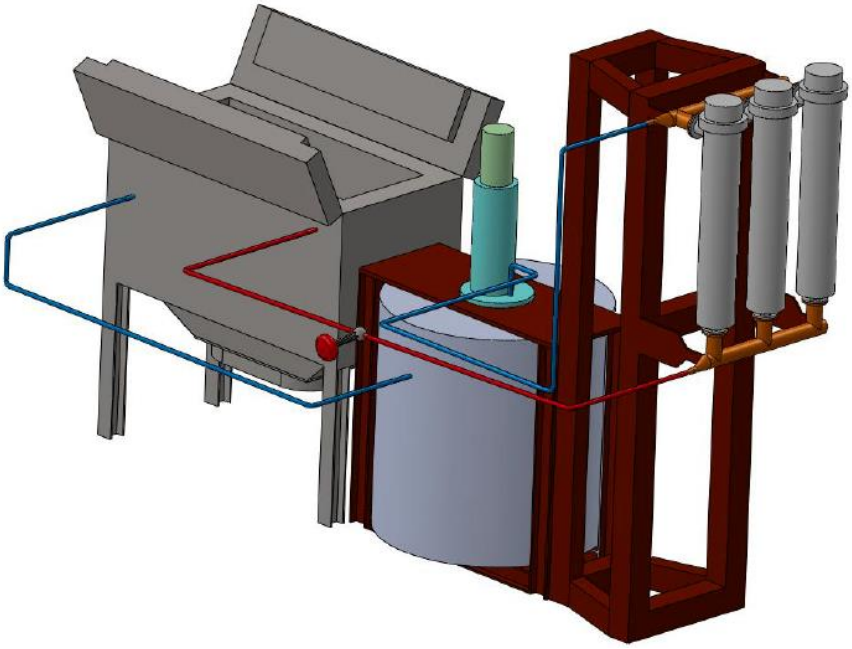

Figure 2.30. Isometric view of the High Temperature Storage Loop Design [47].

The Figure shows many of the aspects of the High Temperature Storage Loop and the way they meet the design goals determined in the scoping phase of the project. The system has a 3. 8m^3 tank topped with an 8.6 kg/s pump. Haynes 230 piping connects this pump to the electric heaters which have the ability to add 600 kWth to the heat transfer fluid. The electric heaters are mounted on a tower that serves the functions of providing altitude for automatic drain back to the tank, but more importantly, a potential support structure for a receiver or other heating system. The heated salt flows through a pressure control valve to the air/HTF cooler. The pressure control valve sets the pressure of the system while the pump speed is used to adjust flowrate. The cooler has insulating doors to prevent excessive thermal loss when there is no heat being added to the system and uses ambient air blown past serpentine tubes containing the flowing HTF. The tank, positioned at the rear of the test unit can be replaced with a power cycle for testing of novel high efficiency power cycle designs. After the cooler/power cycle, the HTF flows back to the tank for storage. Everything in the system is positioned so that the HTF will drain back to the tank when pumping stops. Not shown in the Figure is a vent line that runs from the tank ullage to the top of the heater unit to prevent vacuum when draining back.

2.5.4.2 Tank

The system storage tank has a Haynes 230 inner liner surrounded by insulating firebricks that both support and insulate the tank and its fluid contents before an outer shell of 304H stainless steel. The tank is designed for a 1 atm operating pressure conditions. The system also has overpressure capability and is heated by cal rods affixed to the outside of the liner. The inner liner is connected to the outer shell by bellows that allows for differential thermal expansion between the hot inner liner and the ambient shell. The insulating firebrick that was selected has a very low thermal conductivity which comes at the expense of compressive "crush" strength. However, because the tanks inner liner is not very thick, and because the tank height is not so large, the insulating firebricks have ample strength to handle the load.

2.5.4.3 Pump

The pump included in the design is a Lawrence Pump 1.5 m x 2 m x 12 m which is capable of producing 6.8 kg/s (70 gpm) with a head of about 45m. The pump is a cantilevered pump so that no bearings are required to be submerged in the hot salt. The pump material for this design was primarily Inconel 600, though the material might need to be changed depending on the final choices of heat transfer/molten salt (which may be a fluoride) and the results of materials compatibility testing. Important consideration for a pump of this type is that the lead time for the pump is quoted at 42-46 weeks and a refined pump quote would require another 3 weeks prior to ordering [47]. As experienced with the construction of the 585 °C Molten Salt Test Loop at MSTL, the price and delivery of molten salt pumps are a significant hindrance to the development and fabrication of both test loops like the one proposed here and also of full size storage systems to be installed in power production plants [47].

2.5.4.4 Piping

The piping for the system was chosen based on its ability to contain the pressures and flowrates at the temperature of operation. The pipe is Haynes 230 which has shown reasonable resistance to corrosion in chloride salts and should exhibit good characteristics in both fluoride and carbonate salts as well, though previous testing in these salts is sparse in the literature. The pipe is schedule 40 which will withstand the pressure at the design temperature for the loop. Additionally, the pipe is 1-1/2" nominal diameter pipe, chosen because of the desire to keep flowrates below 10 ft/s to prevent erosion. Because the pipe is relatively thin wall (schedule 40) and of relatively small diameter, the expansion loops may be much smaller without generating excessive stress at the elbows upon heating and subsequent pipe expansion. Also, because the cost of these high-nickel alloys is so significant, it is important to take every opportunity to reduce the amount of material required. In high-nickel pipe, much of the pipe is only available in welded form because of nickel's tendency to work harden [47]. For this loop, the pipe selected is welded seam pipe with a class III rating which defines the cold work required on the weld. Class III pipe is "fully cold reduced" and is the suggested material for highly corrosive materials. If the loop were only going to operate with carbonate salts, it would probably be fine to utilize "cold-bead

worked, fully solution annealed". For the pipe fittings, H230 fittings were not available, so Hastelloy B2 was selected because of its resistance to chloride-containing materials specifically. Like the pipe, the fittings are 1-1/2" schedule 40 and are butt-welded [47].

2.5.4.5 Heaters

The heaters have Incoloy sheath tubular heating elements are flange type heaters. The heaters are rated at 200kW each, but could be supplied with 230kW heating capacity which would then require only 3 heaters to achieve the target goal of 700kW. However, to achieve higher power generation, induction heaters are recommended. The goal of 700 kW was derived from the required heat input to operate the supercritical CO2 turbine loop that exists in the Advanced Nuclear Concepts group at Sandia National Laboratories. Some challenges that would have to be addressed include the flanges on these heaters which are typically standard 150 lb. pipe flanges. Because of the thermal cycling that is typical of a similar test rig and due to the different operational temperatures, where the system would likely exhibit significant stretching of the flange bolts which could lead to leakage during subsequent operation at cooler temperatures. If one can keep the thermal cycling to a minimum, this challenge can be addressed with hot torqueing of the bolts followed by somewhat frequent replacement of the bolts to prevent failure. Even with this methodology to bolt tightening, there is still a concern about the available gasket types and their compatibility with high temperature molten salts. To date, no robust options have been found for this gasket material. Another method of addressing the flanges would try different high temperature flanges. These have seen some success at lower temperature and might operate well at high temperature as well. A third option is to back weld the flange which makes maintenance much harder, but also less necessary. In any case, this is an unresolved issue that must be addressed within R&D. The heaters are attached to Hastelloy B2 headers which are primarily composed of 6" tees with intermediate short spool pieces to achieve appropriate spacing between the heaters for insulation. The heaters hang from the top heater header and the bottom header is free to expand vertically with thermal growth. It is hoped that the same stand that holds the heaters could be used for receiver testing. It would require the addition of some insulation board and foil shielding from stray and reflected flux but supplies a strong base onto which a receiver test could be attached [47].

2.5.5.6 Cooling System

The cooling system is of a design similar to the one installed within the NSTTF MSTL system. The cooler has two fans driven by variable frequency drives, two sets of dampers/louvers that are used to control air flow from natural convection, heating rods to maintain the internal box temperature and to preheat the air at lower temperature cooling conditions, and a set of large insulated doors to keep the heat in the device when the salt is not flowing or does not require any cooling. Like most molten salt high temperature storage system designs, the primary challenge is to keep the fluids molten and moving. Coolers are no exception and spend all non-operating time as heaters to prevent freeze-up on the inside of the finned tubes. The cooler is positioned fairly high off the ground to aid airflow to the fans and to allow for drain back to the tank when the system shuts down [47].

2.5.5.7 Heat Trace

The proposed heat trace is similar to the heat trace used MSTL. This heat trace uses Inconel 600 cable and has sufficient temperature range to allow utilization at these higher temperatures. Because of the potential high operating temperatures, the heat trace requires a conductor along the pipe and an additional but separate return conductor. For a relatively small system like this, and to reduce cost, the heat trace zones will be controlled by manually set local controllers [47].

2.5.5.8 Electrical Equipment

The electrical equipment for this test loop design includes a transformer and switch, motor control center including main circuit breaker and appropriately-sized motor starter. Also included are a Variable Frequency Drive for the pump, an Uninterruptible Power Supply, a main disconnect and electrical panels with breakers [47].

2.5.5.9 Insulation

The insulation for this design is high temperature insulation with a stainless-steel jacket. This configuration is very similar to that used in MSTL. The insulation would not necessarily provide a hand-safe surface, but would instead be sized to prevent excessive heat loss.

2.5.5.10 Controls

The system is designed with a NI Compact RIO controller, extension chassis, and modules for thermocouples, digital inputs and outputs, and analog inputs and outputs (4-20mA). The CompactRIO is a very strategic control system because it functions with the control logic residing on the CompactRIO. Therefore, the programming of the system can be done in a user-friendly windows environment using LabVIEW software, but once downloaded, the system runs in a robust manner independently from the computer. If the computer crashes or is taken off line, the control system will continue to operate in a safe, orderly manner. The system was also designed with a laptop for system control due to its modular, portable nature in the design [47].

Appendix C. Molten Salt Test Loop Images as of September 2017

The following pictures were taken by Richard Sisson on September 2017, to show the current status of the MSTL experiment. A cursory exterior overview shows some weathering, but the degree of disrepair appears minimal, and is due in large part to Albuquerque's arid climate.